Acta Biomaterialia 173 (2024) 167–183

Contents lists available at ScienceDirect

Acta Biomaterialia

journal homepage: www.elsevier.com/locate/actbio

Full length article

Biomechanical characterization of the passive porcine stomach

Clarissa S. Holzer[a], Anna Pukaluk[a], Christian Viertler[b], Peter Regitnig[b], Alexander W. Caulk[c], Matthew Eschbach[c], Elizabeth M. Contini[c], Gerhard A. Holzapfel[a,d,*]

[a] Institute of Biomechanics, Graz University of Technology, Austria
[b] Diagnostic and Research Institute of Pathology, Medical University of Graz, Austria
[c] Surgical Innovations, Medtronic, North Haven, CT, USA
[d] Department of Structural Engineering, NTNU, Trondheim, Norway

ARTICLE INFO

Article history:
Received 13 July 2023
Revised 2 November 2023
Accepted 7 November 2023
Available online 19 November 2023

Keywords:
Porcine stomach
Gastric regions and layers
Biomechanical testing
Histological investigation

ABSTRACT

The complex mechanics of the gastric wall facilitates the main digestive tasks of the stomach. However, the interplay between the mechanical properties of the stomach, its microstructure, and its vital functions is not yet fully understood. Importantly, the pig animal model is widely used in biomedical research for preliminary or ethically prohibited studies of the human digestion system. Therefore, this study aims to thoroughly characterize the mechanical behavior and microstructure of the porcine stomach. For this purpose, multiple quasi-static mechanical tests were carried out with three different loading modes, i.e., planar biaxial extension, radial compression, and simple shear. Stress-relaxation tests complemented the quasi-static experiments to evaluate the deformation and strain-dependent viscoelastic properties. Each experiment was conducted on specimens of the complete stomach wall and two separate layers, mucosa and muscularis, from each of the three gastric regions, i.e., fundus, body, and antrum. The significant preconditioning effects and the considerable regional and layer-specific differences in the tissue response were analyzed. Furthermore, the mechanical experiments were complemented with histology to examine the influence of the microstructural composition on the macrostructural mechanical response and *vice versa*. Importantly, the shear tests showed lower stresses in the complete wall compared to the single layers which the loose network of submucosal collagen might explain. Also, the stratum arrangement of the muscularis might explain mechanical anisotropy during tensile tests. This study shows that gastric tissue is characterized by a highly heterogeneous microstructure with regional variations in layer composition reflecting not only functional differences but also diverse mechanical behavior.

Statement of Significance

Unfortunately, only few experimental data on gastric tissue are available for an adequate material parameter and model estimation. The present study therefore combines layer- and region-specific stomach wall mechanics obtained under multiple loading conditions with histological insights into the heterogeneous microstructure. On the one hand, the extensive data sets of this study expand our understanding of the interplay between gastric mechanics, motility and functionality, which could help to identify and treat associated pathologies. On the other hand, such data sets are of high relevance for the constitutive modeling of stomach tissue, and its application in the field of medical engineering, e.g., in the development of surgical staplers and the improvement of bariatric surgical interventions.

1. Introduction

Gastrointestinal (GI) health problems are among the leading causes of morbidity and cost-intensive medical conditions in industrialized countries [1,2]. In the USA alone, up to 70 million people are affected by GI diseases each year [3,4], resulting in over-

* Corresponding author at: Institute of Biomechanics, Graz University of Technology, Austria.
E-mail address: holzapfel@tugraz.at (G.A. Holzapfel).

https://doi.org/10.1016/j.actbio.2023.11.008

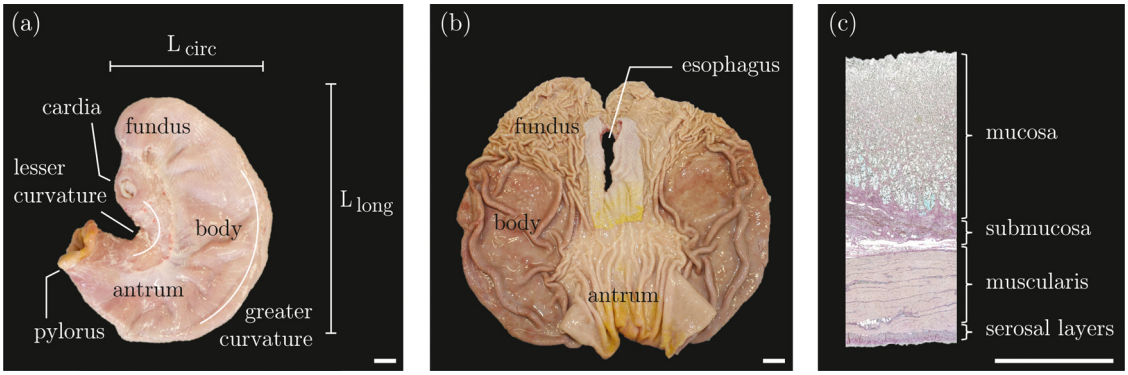

Fig. 1. Regions and layers of the porcine stomach: (a) exterior view of an emptied, intact stomach to measure its dimensions in the circumferential and longitudinal direction, L_{circ} and L_{long}, and the optical differentiation of the gastric regions, i.e., fundus, body, and antrum; (b) interior view of the stomach cut open along the greater curvature; (c) exemplary histological slide of the cross-section of the SW showing all four main layers: mucosa, submucosa, muscularis, and serosa. The white scale bars correspond to 2 cm in (a) and (b), and 2 mm in (c).

all direct healthcare costs of about $136 billion per year [5]. These costs do not include indirect costs related to decreased labor productivity, employee turnover or sick leave, or costs related to the soaring share of the population suffering from obesity. According to recent estimates, more than a third of the USA adult population meets criteria for obesity [6], costing the healthcare system approximately $173 billion per year [7]. Overweight and obesity are not only associated with multiple comorbidities such as reflux disease, diabetes mellior or hypertension, but also with an increased risk of cancer [8,9]. It is noteworthy that stomach cancer has one of the lowest five-year survival rates of all types of cancer worldwide [10]. In 2020, more than a million new cancer cases worldwide can be attributed to it [11]. Although the incidence and mortality rates of gastric cancer in Europe and North America have decreased significantly since the 1930s [12], stomach cancer is currently the most common cancer and the leading cause of cancer-related death in several Asian countries [11].

Gastrectomies have been shown to be a successful surgical intervention for long-term weight reduction in obese patients [13,14] and for complete removal of gastric tumor lesions [15–17]. These surgeries are closely linked to the anatomy, microstructure, and mechanics of the stomach. Moreover, such surgeries could benefit greatly from material models of the stomach wall (SW), which could support the development of medical tools [18] and preoperative planning [19]. Accurate and reliable material models require experimental data sets that provide information about the microstructure and mechanics of the stomach.

The stomach is a vital part of the GI tract and is positioned between the esophagus and the intestines. The bean-shaped muscular hollow organ has three functions [20]: (i) to accommodate the ingested food and gases that are passed from the esophagus through the inlet orifice, i.e. the cardia; (ii) to chemically and mechanically reduce the size of the solid food particles to a digestible size by grinding the bolus by peristaltic muscle movements and mixing it with gastric juices; (iii) to empty the chyme in a controlled way into the duodenum through the outlet orifice, i.e. the pylorus, for further digestion and absorption. These three main tasks are fulfilled by the functional and regional division of the stomach into three regions, namely fundus, body and antrum (see Fig. 1(a) and (b)).

Like most parts of the GI tract, the stomach features a complex multi-layered wall with a distinct microstructure. As shown in Fig. 1(c), the four main layers of the SW are the mucosa, submucosa, muscularis, and serosal layer [21]. The mucosa, the innermost layer, consists of a multitude of gastric glands, the lamina propria, and the muscularis mucosae, and forms distinctive folds called rugae, which flatten out during ingestion and digestion of food. The distribution, orientation, and dimensions of the rugae are strongly region-dependent, while they are only a few millimeters high, dispersed and tightly packed in the fundus, they are up to one centimeter high, rather oriented along the longitudinal direction and far apart from one another in the body. The submucosa, a thick, loose collagen network that contains blood and lymphatic vessels, among other things, enables the mucosa to move largely independently of the muscular layer [22,23]. The muscular layer is arranged in at least two interwoven strata consisting of muscle bundles enveloped by sheets of collagenous extracellular matrix. The outer stratum features longitudinally aligned muscle fibers, while the muscle fibers of the inner stratum are mostly oriented circumferentially. The muscularis is covered by the serosal layer, which contains a collagen network (also called subserosa) and a mesothelium responsible for reducing friction in the abdominal cavity.

Hardly any literature has been documented about the passive stomach mechanics [24]. However, there are some studies that have been conducted at either the organ level or the tissue level. The organ-level studies led to a deeper understanding of gastric flow rate and pressure through inflation tests [25–28]. However, they could not directly evaluate the layer- and region-specific properties of the SW needed for the development of material models. Also, an organ-level study in compression mode [29] did not examine regional differences in stomach tissue, but provided an estimation of the similarity and disparity of the stomach compared to other abdominal organs. An effective way to achieve a comprehensive understanding of layer-, direction-, and region-specific characteristics is to conduct tissue-level experiments with multiple loading modes. To the best of the authors' knowledge, previous tissue-level experiments include uniaxial extension [30–37], biaxial extension [38,39], and compression tests [37], but not shear tests. Among the aforementioned studies, only Friis et al. [37] performed tissue-level experiments with more than one loading mode. Most studies included only one strain rate [30,31,34,38,39]. The region-specific properties of the stomach were evaluated by most research groups [31,33–39], but only some of them showed layer-specific properties [31,33,37,39]. Another important aspect of tissue mechanics is tissue viscoelasticity, which only a few research groups have examined [29,33,35–37]. Furthermore, the mechanical data are rarely substantiated by histological study and microstructural analysis [39].

The limited data availability significantly affects the applicability of the measurement data in constitutive tissue modeling and thus a comprehensive understanding of tissue mechanics. Therefore, this study aimed at obtaining a mechanical data set that includes: (i) multiple loading modes such as radial compression, pla-

Table 1
Average stomach dimensions in the longitudinal, L_{long}, and circumferential direction, L_{circ}, and weight, W (mean ± standard deviation).

	L_{long} [cm]	L_{circ} [cm]	W [g]
All stomachs	23.1 ± 1.7	10.8 ± 1.4	543 ± 60
Male	23.8 ± 1.6	11.3 ± 1.4	579 ± 60
Female	22.5 ± 1.7	10.4 ± 1.3	508 ± 36

nar biaxial extension, and simple shear; (ii) two strain rates for relevant loading modes; (iii) region and layer-specific properties; (iv) analysis of the tissue viscoelasticity. Furthermore, the mechanical data were complemented by a microstructural examination to deepen the understanding of the stomach and to pave the way for a realistic constitutive model for biomedical engineering.

2. Methods

2.1. Stomach specimens

For this study, ten ($n = 10$) intact stomachs were obtained from domestic pigs (*sus domesticus*, five male and five female, approximately six months old, weight between 100 and 120 kg). They were transported from the local slaughterhouse to the laboratory in less than 30 min after the animal has been sacrificed. To prevent tissue dehydration, the stomachs were stored in phosphate-buffered saline solution (PBS) with pH 7.4 during transport. The stomachs were then rinsed with water to remove any remnants of the chyme and gastric juices. Subsequently, the stomachs were measured (see Fig. 1(a)) and weighed. Estimated average lengths in the longitudinal, L_{long}, and circumferential direction, L_{circ}, and average weights W of the deflated stomachs are summarized in Table 1.

After removal of the lesser and greater omentum and outer fatty tissue, the stomachs were cut open along the greater curvature and rinsed again with water. The coloration, amount, and size of the gastric rugae of the mucosal layer allowed a clear differentiation between the three stomach regions, i.e., fundus, body, and antrum (see Fig. 1(b)). On this basis, stomach regions were separated and frozen in PBS at −20°C for later mechanical experiments and histological investigation to minimize tissue deterioration due to proteolysis. All samples were frozen within 2 h of arrival at the laboratory.

2.2. Sample preparation

After thawing overnight at 4°C, each sample was placed in cardioplegic solution (CPS) containing dissolved 2,3-butanedione monoxime (BDM, 30 mM per liter CPS) for at least 1 h prior to testing to ensure the passiveness of the smooth muscle cells of the SW and to acclimatize to room temperature (approx. 22°C). Due to its unphysiologically high concentration of potassium, CPS leads to a depolarization of the cell membrane, which in turn leads to muscle contractions. As a result, intracellular calcium is sequestered, the cell relaxes again and repolarization is hindered by the increased potassium concentration, which leads to electromechanical decoupling [40,41]. Further, multiple studies have shown that BDM inhibits myosin light chain reactions in cardiac and smooth muscles, directly reducing force generation at the cross-bridge level and largely preventing muscle contraction [42–45].

All mechanical tests were conducted for each region. In all three regions, complete SW samples, samples of the mucosa (and a smaller remainder of the submucosal layer), and samples from the muscularis and serosal layer were tested. Based on previous studies [38,39] it was assumed that the anterior and posterior halves of the stomach are structurally and mechanically symmetrical. All histological and shear test samples were therefore cut from the anterior, and all compression and tensile test samples from corresponding areas of the posterior half of the stomach. Because of the natural folding of the mucosal layer, sample positions varied slightly from stomach specimen to another. In particular, the areas of the naturally flat mucosal layer were excised for test purposes in order to reduce the influence of tissue flattening during the experiments as much as possible. Square samples of 20 mm edge length were cut for the biaxial tensile tests and square samples of 8 mm edge length were prepared for simple shear and radial compression tests. For histological investigations, rectangle samples of 4×8 mm were cut. The samples used for the layer-specific measurements were taken from tissue adjacent to the samples used for testing the complete SW. The edges of each square and rectangle sample were kept parallel with and perpendicular to the greater curvature. The initial thickness T of each sample was measured optically using a video extensometer [46] and later used for postprocessing of the mechanical data of the respective sample.

2.3. Histological investigations

Five complete SW samples of all three regions were fixed with 4% formaldehyde. The samples were then embedded in paraffin and cut into 3 to 5 µm thick slices using the Microm HM 430 (Microm, Walldorf/Baden, Germany). A combination of two contrast agents, i.e. Elastica van Gieson and Alcian blue, was used to distinguish the different microstructural constituents. Elastica van Gieson stains the muscle bundles in a yellowish tint, collagen fibers in magenta to dark red, and cell nuclei in dark blue to black. Alcian blue stains mucin turquoise [47]. The detailed staining protocol can be found in the supplementary material. The histological slices were scanned with the digital slide scanner PANNORAMIC 1000 (3DHISTECH, Budapest, Hungary).

2.4. Mechanical testing

2.4.1. Biaxial extension

A planar biaxial extension testing machine for soft biological tissues was used to conduct the stretch-controlled biaxial tensile experiments, see Sommer et al. [48,49]. According to a template proposed in [50], the samples were hooked uniformly at five positions along each 20 mm long edge to ensure a uniform strain distribution in the center of the sample [51,52]. Along each edge, the set of hooks was connected by a suture cord, allowing the hooks to move along the cord to reduce shear effects during the test (Fig. 2). A video extensometer tracked the current in-plane deformation during the test from the speckle pattern applied with a black ink (BioGnost Ltd., Zagreb, Croatia) to the sample surface. After mounting and submerging the samples in CPS with dissolved BDM, a preload of 10 mN was applied in both directions to avoid the weight effect. This state was defined as the reference configuration at $\lambda = 1.0$.

A total of $n = 90$ samples, i.e. ten samples per region and layer combination, were subjected to the following test protocol, starting with five equibiaxial preconditioning cycles up to $\lambda = 1.1$. The number of preconditioning cycles was chosen based on preliminary studies. Stretch ratios of 1 : 1, 4 : 3, 3 : 4, 2 : 1, and 1 : 2 between the circumferential and longitudinal directions were then applied to each sample at a speed of 3 mm/min, with the maximal stretch of 1.1. The measurement protocol was repeated with stretch increments of $\Delta\lambda = 0.1$ until tissue failure.

2.4.2. Radial compression

The radial compression tests were also conducted in the planar biaxial extension testing machine [48,49], which was newly

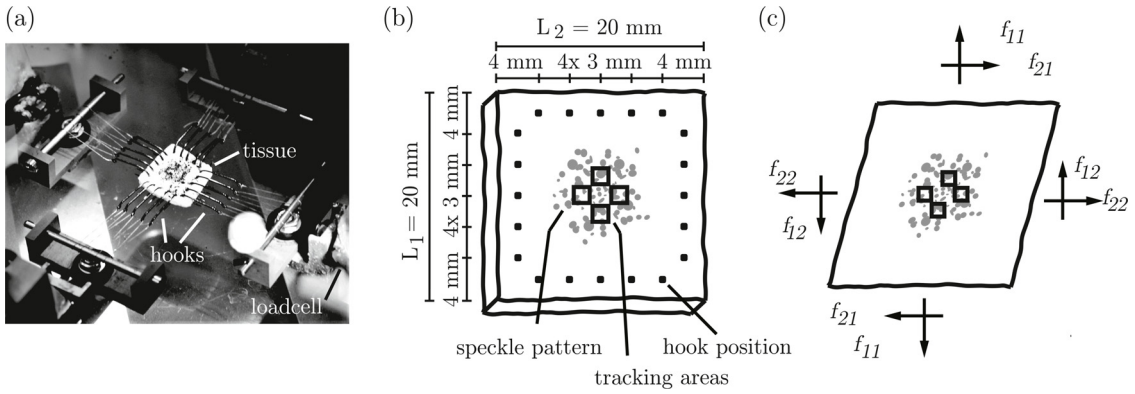

Fig. 2. Experimental setup: (a) square-shaped gastric tissue mounted in the biaxial testing machine; (b) an illustration of the sample geometry, hook positions, and tracking areas; (c) forces acting on the sample during biaxial extension test, where f_{1i} sum up to f_{circ} and f_{2i} sum up to f_{long}.

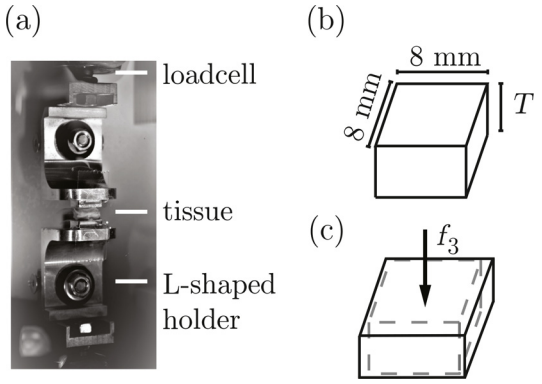

Fig. 3. Experimental setup: (a) square cuboid-shaped gastric tissue mounted in the biaxial testing machine; (b) illustration of the sample geometry in reference configuration; (c) deformed configuration during radial compression testing.

equipped with suitable L-shaped specimen holders (see Fig. 3(a)). Double-faced adhesive tape and square pieces of sandpaper with an average particle diameter $d_{p,avg} = 120$ µm were mounted to both opposed holders. A thin coat of cyanoacrylate adhesive was applied to the sandpaper to fix the sample between the holders. To harden the adhesive, a preload of 10 mN was applied in the radial direction for 120 s. After this curing time, the holders were moved back to the originally measured sample thickness T using a video extensometer. The sample was then humidified with the CPS. This state was defined as the reference configuration.

All region and layer-dependent radial compression tests were performed under quasi-static conditions ($v = 3$ mm/min) for three different stretch levels $\lambda = \{0.8, 0.6, 0.4\}$. A new sample was used for each loading case in order to exclude the influence of possible microstructural damage due to previous compressions. This resulted in a total of $n = 270$ samples. Each sample was subjected to five preconditioning cycles up to the respective stretch level of the subsequent measurement cycle. The number of preconditioning cycles was based on the preliminary studies.

In addition, the same number of relaxation tests was conducted on separate samples to account for the viscoelasticity of the tissue. For this reason, a fast compressive step up to $\lambda = \{0.8, 0.6, 0.4\}$ at a ramp speed of $v = 100$ mm/min was applied and the mechanical response was recorded over a period of 10 min.

2.4.3. Simple shear

For the simple shear tests, double-faced adhesive tape and square pieces of sandpaper ($d_{p,avg} = 120$ µm) were mounted to both specimen holders. Each sample was glued to the upper holder using cyanoacrylate adhesive and inserted into the triaxial testing device [48,49,53] as shown in Fig. 4(a). A thin layer of glue was then applied to the lower specimen holder and the sample was slowly lowered until a radial preload of 10 mN was reached. This position was held for a hardening period of 120 s. Afterward, the sample was unloaded and humidified with CPS. This state was defined as the reference configuration.

Under quasi-static conditions ($v = 3$ mm/min), region- and layer-dependent simple shear tests along the longitudinal and circumferential direction were performed for two different maximum strain levels $\gamma = \{0.2, 0.4\}$. According to the preliminary studies, two preconditioning cycles were sufficient to ensure a repeatable and comparable tissue response for each sample type. The strain level of the preconditioning cycles was identical to the one of the subsequent measurement cycles.

Furthermore, relaxation tests in simple shear mode were conducted to evaluate the tissue viscoelasticity. These consisted of a fast shear step up to $\gamma = \{0.2, 0.4\}$ with a ramp speed of $v = 100$ mm/min and the recording of the mechanical response over a period of 10 min. To rule out the influence of possible micro- and macroscopic tissue damage due to prior tests, a new sample was used for each shear level and for the quasi-static and relaxation tests, resulting in a total of $n = 360$ samples.

2.5. Data analysis

2.5.1. Biaxial extension

Based on the video extensometer data at the four marker positions, the following deformation gradient is computed assuming tissue incompressibility and homogeneous deformations within the central tracking area, i.e. in matrix notation

$$[\mathbf{F}] = \begin{bmatrix} \lambda_1 & \gamma_1 & 0 \\ \gamma_2 & \lambda_2 & 0 \\ 0 & 0 & \lambda_3 \end{bmatrix}, \tag{1}$$

with the following stretches

$$\lambda_1 = \frac{\partial u_1}{\partial X_1} + 1, \qquad \lambda_2 = \frac{\partial u_2}{\partial X_2} + 1, \qquad \text{and} \qquad \lambda_3 = \frac{1}{\lambda_1 \lambda_2 - \gamma_1 \gamma_2}, \tag{2}$$

and in-plane shear deformations

$$\gamma_1 = \frac{\partial u_1}{\partial X_2}, \qquad \text{and} \qquad \gamma_2 = \frac{\partial u_2}{\partial X_1}. \tag{3}$$

Here λ_i define the stretches, γ_i the amount of in-plane shear, u_i the displacements and X_i the reference coordinates. Knowledge of the deformation gradient $\mathbf{F}$ together with the measured forces in the

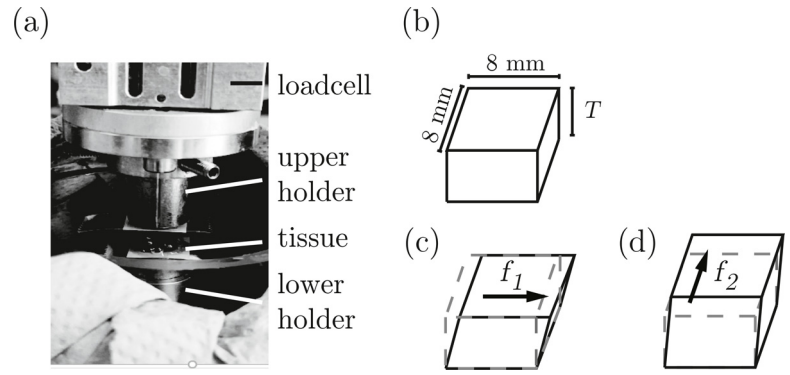

Fig. 4. Experimental setup: (a) square cuboid-shaped gastric tissue mounted in the triaxial testing machine; (b) illustration of the sample geometry in reference configuration; (c) and (d) deformed configurations during simple shear testing along the circumferential and longitudinal direction, respectively ($f_{\text{circ}} = f_1$ and $f_{\text{long}} = f_2$).

circumferential and longitudinal direction, f_{circ} and f_{long}, respectively, and the dimensions of the reference configuration allowed the estimation of the Cauchy normal stresses. Thus,

$$\sigma_{11}(\lambda_1, \gamma_1) = \lambda_1 \frac{f_{11}}{TL_2} + \gamma_1 \frac{f_{21}}{TL_1} := \sigma_{\text{circ}},$$
$$\text{and} \quad \sigma_{22}(\lambda_2, \gamma_2) = \lambda_2 \frac{f_{22}}{TL_1} + \gamma_2 \frac{f_{12}}{TL_2} := \sigma_{\text{long}}. \tag{4}$$

Here f_{1i} sum up to the measured circumferential force f_{circ} and f_{2i} sum up to the measured longitudinal force f_{long}. The parameter T defines the initial sample thickness and L_i the sample length and width. In several studies on the GI-tract [38,54] and other fiber-reinforced soft tissues [55,56] it was assumed that shear effects in planar biaxial extension are negligible. For this reason, the shear forces were assumed to be negligible in the following assessment. This leads to the second part of both equations being set to zero, resulting in $\sigma_{\text{circ}} = \sigma_{11}(\lambda_1)$ and $\sigma_{\text{long}} = \sigma_{22}(\lambda_2)$.

2.5.2. Radial compression

Assuming that the gastric tissue is incompressible and deforms homogeneously during uniaxial, unconfined compression (see Fig. 3(b) and (c)), the deformation gradient is

$$[\mathbf{F}] = \begin{bmatrix} \lambda_1 & 0 & 0 \\ 0 & \lambda_2 & 0 \\ 0 & 0 & \lambda_3 \end{bmatrix}, \tag{5}$$

with the relations between the principal stretches, i.e.

$$\lambda_1 = \lambda_2 = \frac{1}{\sqrt{\lambda}}, \qquad \text{and} \qquad \lambda_3 = \lambda. \tag{6}$$

The stretch $\lambda = 1 + \Delta z/T$ was computed with respect to the displacement Δz from the reference configuration and the unloaded thickness T of the sample. The first Piola-Kirchhoff stress P_3 was calculated by dividing the measured force f_3 by the unloaded cross-sectional area A_{12} of the sample in the reference configuration according to

$$P_3 = \frac{f_3}{A_{12}} = \frac{f_3}{L_1 L_2}. \tag{7}$$

2.5.3. Simple shear

In simple shear, the deformation gradient $\mathbf{F}_{31}$ in the radial-circumferential mode (Fig. 4(c)) and in the radial-longitudinal $\mathbf{F}_{32}$ (Fig. 4(d)) mode is as follows

$$[\mathbf{F}_{31}] = \begin{bmatrix} 1 & 0 & \gamma \\ 0 & 1 & 0 \\ 0 & 0 & 1 \end{bmatrix} \qquad \text{and} \qquad [\mathbf{F}_{32}] = \begin{bmatrix} 1 & 0 & 0 \\ 0 & 1 & \gamma \\ 0 & 0 & 1 \end{bmatrix}, \tag{8}$$

where γ is the amount of shear, defined as the ratio between the relative displacement of two parallel planes within a sample and the distance separating them, see Fig. 4. This corresponds to a combination of pure shear and rotation and thus leads to a non-symmetric deformation gradient $\mathbf{F} = \mathbf{RU}$, where $\mathbf{R}$ is a measure of the local rotation tensor and $\mathbf{U}$ is the right stretch tensor [57,58]. Therefore, some line elements stretch while others contract depending on their orientation. The principal stretches are given by the positive square roots of the eigenvalues of the right Cauchy-Green tensor $\mathbf{C} = \mathbf{U}^{\mathrm{T}}\mathbf{U}$ and result in

$$\lambda_1 = \lambda_2 = \pm\frac{\gamma}{2} + \sqrt{1 + \frac{\gamma^2}{4}} \qquad \text{and} \qquad \lambda_3 = 1. \tag{9}$$

The shear stresses were computed by dividing the recorded force in the direction of the shear by the initial area, i.e.

$$\tau_1 = \frac{f_1}{L_1 L_2} \qquad \text{and} \qquad \tau_2 = \frac{f_2}{L_1 L_2}. \tag{10}$$

2.6. Statistical analyses

Statistical analyses of the experimental data were conducted to shed light on possible regional, directional, and layer-specific differences in the obtained stress-strain responses of porcine gastric tissue. In order to distinguish between normal and non-normal distributions of the data obtained, a Shapiro-Wilk test was carried out, which is especially suitable for small sample sizes. Since the vast majority of the data were non-normally distributed, a Mann–Whitney U-test was used for the data analyses. Parameter differences between the different regions, layers, and directions were evaluated, if the sample size was sufficiently high ($n \geq 10$), and considered statistically significant if the p-value was less than 0.05, corresponding to a confidence of 95%. All statistical tests were performed using MATLAB 2021a (The MathWorks, Inc., Natick, Massachusetts, USA).

3. Results

3.1. Histological investigations

The histological investigations showed a highly heterogeneous tissue composition in the examined stomach layers and regions (Fig. 5). The thickness of each layer and the complete wall was strongly region dependent. The SW of the fundus was thinnest at an average of 5.0 ± 0.2 mm, followed by the body with 5.2 ± 0.1 mm and the antrum with 8.1 ± 0.3 mm. Interestingly, the muscularis and mucosa were about the same thickness in the body. On the contrary, the muscularis is thicker than all other layers combined in the fundus and antrum. In addition, the fundic submucosa

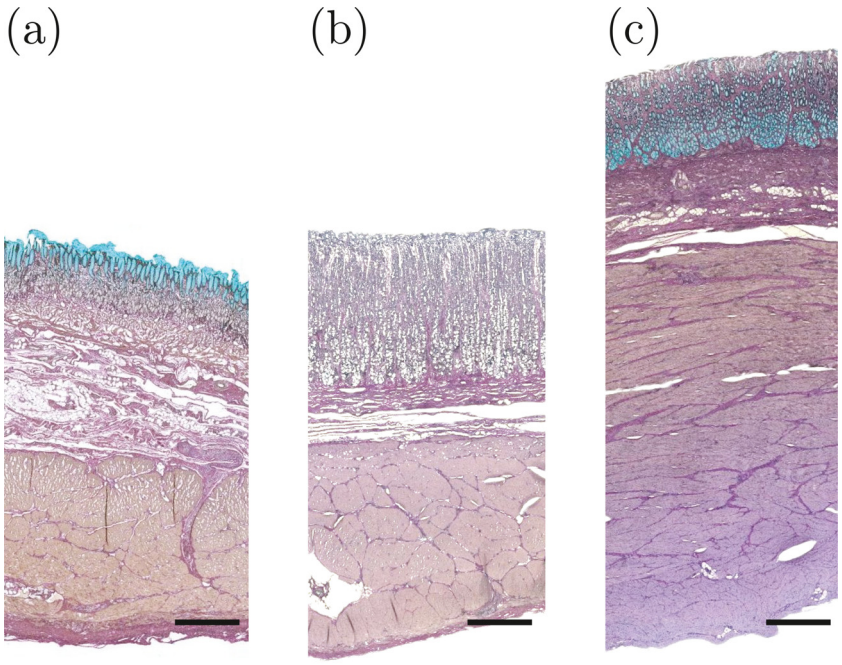

Fig. 5. Exemplary histological slides of a radial-circumferential cross-section of each region: (a) fundus; (b) body; (c) antrum. The tissue was stained using a combination of Elastica van Gieson and Alcian blue, resulting in turquoise coloration of the mucus in the mucosal glands, a yellowish tint of the muscles, magenta to red-stained collagen fibers, and dark blue to black cell nuclei. The black scale bars correspond to 1 mm.

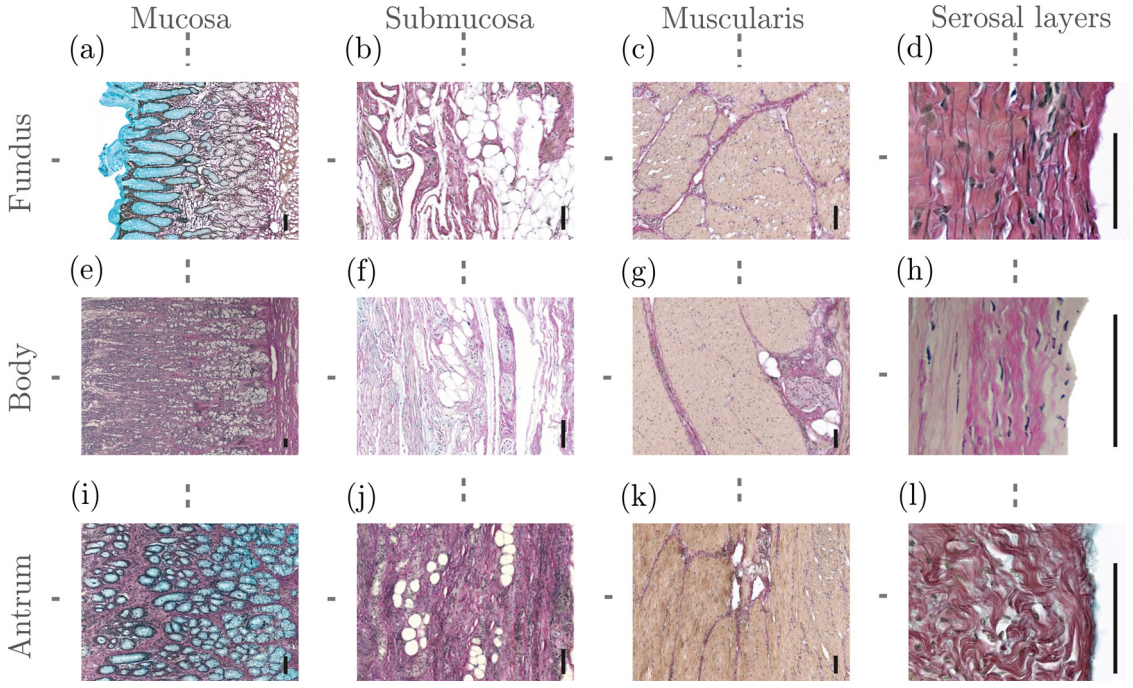

Fig. 6. Layer-specific close-ups of exemplary histological slides with radial-longitudinal cross-sections of each region: (a)–(d) fundus; (e)–(h) body; (i)–(l) antrum. The tissue was stained with a combination of Elastica van Gieson and Alcian blue. The black scale bars correspond to 100 µm.

was clearly thicker compared to the body and antrum, and contained more adipose tissue, see Fig. 6. The serosa is slightly thicker in the fundus and antrum than in the body.

The composition of the layers also differed regionally (Fig. 6). The innermost part of the tunica mucosa consists of the gastric glands, which empty into the superficial pits. Foveolar cells line the necks of the pits and the mucosal surface and produce mucus (shown in turquoise in Figs. 5(a)–(c) and 6(a),(e) and (i)), which protects the stomach from self-digestion. While the fundus and the body mostly contained mainly radially aligned, straight oxyntic glands lined by parietal cells and underlying chief cells, the antrum presented mainly coiled, mucinous glands, similar to the corresponding regions in the human stomach [59,60]. These mucinous antral glands were often clustered with collagen and muscle fibers, similar to stomachs of human [21] and babirusa stomachs [47]. Both, the lamina propria and the muscularis mucosae showed a fairly homogeneous structure and thickness throughout the stomach.

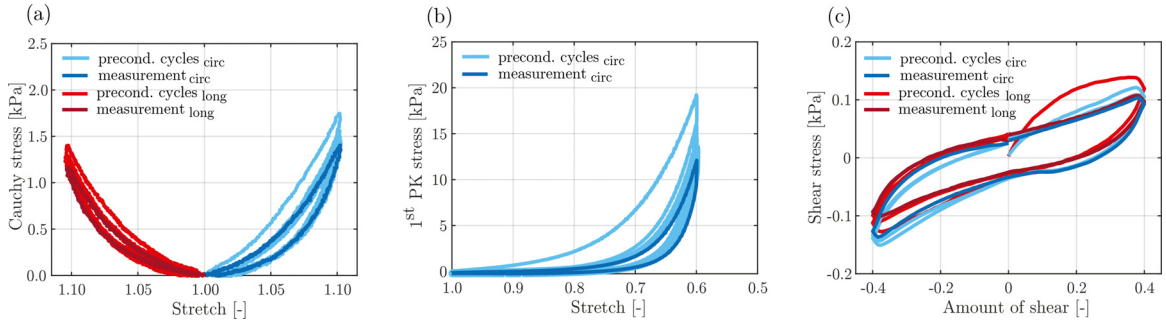

Fig. 7. Representative preconditioning behavior of the complete SW of the body during the three different loading modes: (a) equibiaxial planar extension; (b) radial compression; (c) simple shear. The preconditioning cycles are shown in light-colored curves, the measurement curves in dark-colored curves. In (a) and (c), the red and blue curves represent the tissue response along the longitudinal and the circumferential direction, respectively.

Depending on the gastric region, not all three strata of the muscularis are equally developed. While all three strata of the muscularis layer are visible in most of the histological slides of the body and antrum, the fundic muscularis is often only composed of the circular and longitudinal strata. In the body and antrum, the main stratum is the circular stratum, and the thickness of the longitudinal stratum is only a small fraction of the circular stratum. In the fundus, on the other hand, the circular and longitudinal strata are about the same thickness. Sometimes the muscle strata are separated by blood vessels and nerves and ganglion cells that form the Auerbach-Plexus. While the strata arrangement regionally varies, the general tissue composition of each stratum is the same: densely packed muscle fiber bundles enveloped by collagen fibers (see Fig. 6(c),(g) and (k)).

For high-resolution versions of Figs. 5 and 6, the reader is referred to the Supplementary Material (see Figs. S1 and S2). Figure S1 contains layer-specific partitions for each region and Fig. S2 includes markers for various structural elements.

3.2. Preconditioning behavior

In general, gastric tissue exhibited a highly nonlinear stress-strain relationship with notable hystereses related to energy dissipation during the quasi-static loading-unloading cycle. In all mechanical tests, there was significant preconditioning and tissue softening between the first and second loading cycle (see Fig. 7). The initial hysteresis was far larger than the following for all three loading modes. It is noteworthy that the initial loading in simple shear occasionally showed a convex behavior while all subsequent loadings featured concave stress-strain relationships. The hystereses curves of the last preconditioning cycle and the measurement cycle were almost identical, indicating that there is no further energy loss.

3.3. Biaxial extension testing

The samples were biaxially stretched until tissue failure occurred, predominantly at one of the hooking positions. The complete list of the maximum stretch reached by each sample is presented in Table 2. Due to the different extensibility within each sample type, stretches were only considered if all measurement cycles were successfully completed by at least 50% of the samples. On average, samples of the fundus were stretched the farthest (although not statistically significant, $p < 0.06$), followed by the antrum and body, except for the mucosa samples, which could be stretched farther in the antrum than the other regions ($p < 0.04$). The mucosa samples were prone to failure at lower (although not statistically significant, $p < 0.08$) stretches than the muscularis and the complete SW in the fundus and body.

The equibiaxial tensile tests showed various regional and layer-specific tissue properties (see Fig. 8; see also Fig. S3 in the Supplementary Material S3 for an example of the non-equibiaxial tensile tests). It is remarkable that only the lowest stretch, $\lambda = 1.1$, was reached for all regions and layers. Thus, all regions and layers on this lowest stretch can be compared. All layers, i.e. the complete SW, the mucosa, and the muscularis, experienced the highest median stresses in the body and the lowest in the antrum at a stretch $\lambda = 1.1$ ($p < 0.01$). For most body and antrum samples, the complete SW showed lower stresses compared to the single layers ($p < 0.08$). Interestingly, the stresses of the complete SW were comparable to those of the muscularis in the fundus and body, but not in the antrum. In the fundus and in the body, the mucosa showed the highest stresses and variability between all layers tested ($p < 0.04$).

In general, the gastric tissue exhibited isotropic behavior at low stretches, but exhibited some degree of anisotropy in all regions at higher stretches. Interestingly, the complete SW showed higher median stresses along the circumferential direction in the fundus and along the longitudinal direction in the body and antrum (compare Fig. 8(a)–(c)). Higher median stresses were found for the mucosa along the longitudinal direction in the antrum, while the mucosa of the fundus and body exhibited more isotropic behavior with equibiaxial extension, see Fig. 8(d)–(f). The muscularis of the fundus and body exhibited higher stresses along the longitudinal direction, while those of the antrum showed higher stresses in the circumferential direction, see Fig. 8(g)–(i).

3.4. Radial compression testing

The radial compression tests revealed that most body samples exhibited a stiffer (although not statistically significant) mechanical response compared to the fundus and antrum samples (Fig. 9). This observation was made for each of the compression levels and for the muscularis as well as the complete SW (muscularis: $p < 0.31$; complete SW: $p < 0.45$). The measurements of the body samples also presented more variability between each measurement curve and higher residual stresses upon unloading. Among the body samples, all layers tested showed comparable median stresses ($p > 0.57$ at $\lambda = 0.4$). Contrary to the body samples, both fundus and antrum samples showed lower stresses in the complete SW compared to the single layers (muscularis: $p < 0.48$, and mucosa: $p < 0.14$). In the antrum, the stress of each single layer nearly doubled the stresses of the complete SW at $\lambda = 0.4$, see Fig. 9(c),(f), and (i). However, in the fundus, the mucosal layer exhibited a higher stress than the muscularis (and the complete SW) for all three compression levels (compare Fig. 9(a),(d), and (g); $p < 0.12$). Generally, a linear behavior could be observed un-

Table 2
The maximum regional stretches λ_{max} are reached with planar biaxial extension of the complete stomach wall (SW), mucosa (MUC), and muscularis (MUS) of each specimen, as well as the maximum evaluated stretch per region and layer combination $\lambda_{max\text{-}eval}$.

	Maximum stretch before failure λ_{max} [-]								
	Fundus			Body			Antrum		
Specimen	SW	MUC	MUS	SW	MUC	MUS	SW	MUC	MUS
SP 1	1.2	1.1	1.4	1.3	1.2	1.1	1.3	1.3	1.2
SP 2	1.3	1.2	1.4	1.1	1.1	1.4	1.2	1.3	1.1
SP 3	1.3	1.2	1.3	1.1	1.1	1.3	1.3	1.3	1.2
SP 4	1.3	1.2	1.4	1.1	1.1	1.2	1.4	1.2	1.2
SP 5	1.4	1.2	1.4	1.2	1.2	1.1	1.3	1.3	1.2
SP 6	1.3	1.2	1.3	1.1	1.1	1.1	1.3	1.2	1.3
SP 7	1.4	1.1	1.4	1.2	1.1	1.2	1.3	1.2	1.2
SP 8	1.4	1.2	1.4	1.2	1.1	1.2	1.3	1.2	1.3
SP 9	1.4	1.1	1.4	1.2	1.1	1.2	1.3	1.3	1.3
SP 10	1.4	1.1	1.3	1.1	1.1	1.2	1.3	1.3	1.1
$\lambda_{max\text{-}eval}$	1.4	1.2	1.4	1.2	1.1	1.2	1.3	1.3	1.2

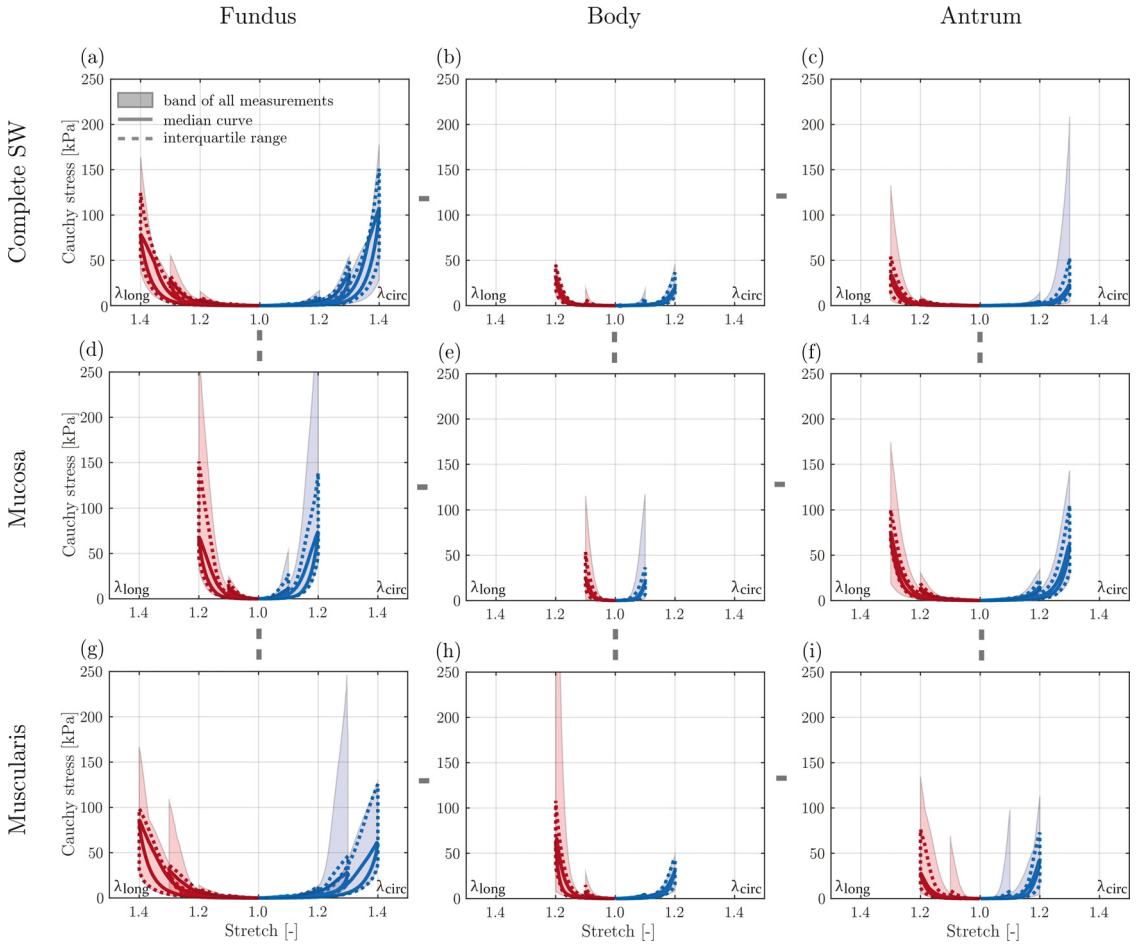

Fig. 8. Region-, layer-, and direction-dependent stress-stretch behavior during the final cycles of quasi-static equibiaxial extension up to a stretch of $\lambda = \{1.1, 1.2, 1.3, 1.4\}$. The blue and red solid curves describe the median of the tissue response in the circumferential and longitudinal direction, respectively. The dashed curves depict the data's interquartile range, and the shaded areas include all measurement curves. A minimum of $n = 5$ samples per testing condition was considered depending on their failure stretch.

til $\lambda = 0.65$, which was then followed by an exponential section of the stress-stretch curves.

3.5. Simple shear testing

The simple shear tests showed that the complete SW experienced the highest shear stresses in the fundus, followed by the body and antrum (although not statistically significant with $p < 0.21$; see Fig. 10 for $\gamma = 0.4$ and Fig. S4 for $\gamma = 0.2$). The mucosal layer showed similar results ($p < 0.23$). However, the mechanical response of the muscularis in the fundus and in the body was similar ($p > 0.67$). The muscularis of the antrum showed statistically significantly lower shear stresses ($p < 0.04$). The fundus also showed the highest variability among the single measurements. For each region, the shear stresses of the complete SW were statistically significantly lower than those of the single layers ($p < 0.01$). Between the single layers, the mucosa showed the greatest shear stresses in the individual regions ($p < 0.06$). It is re-

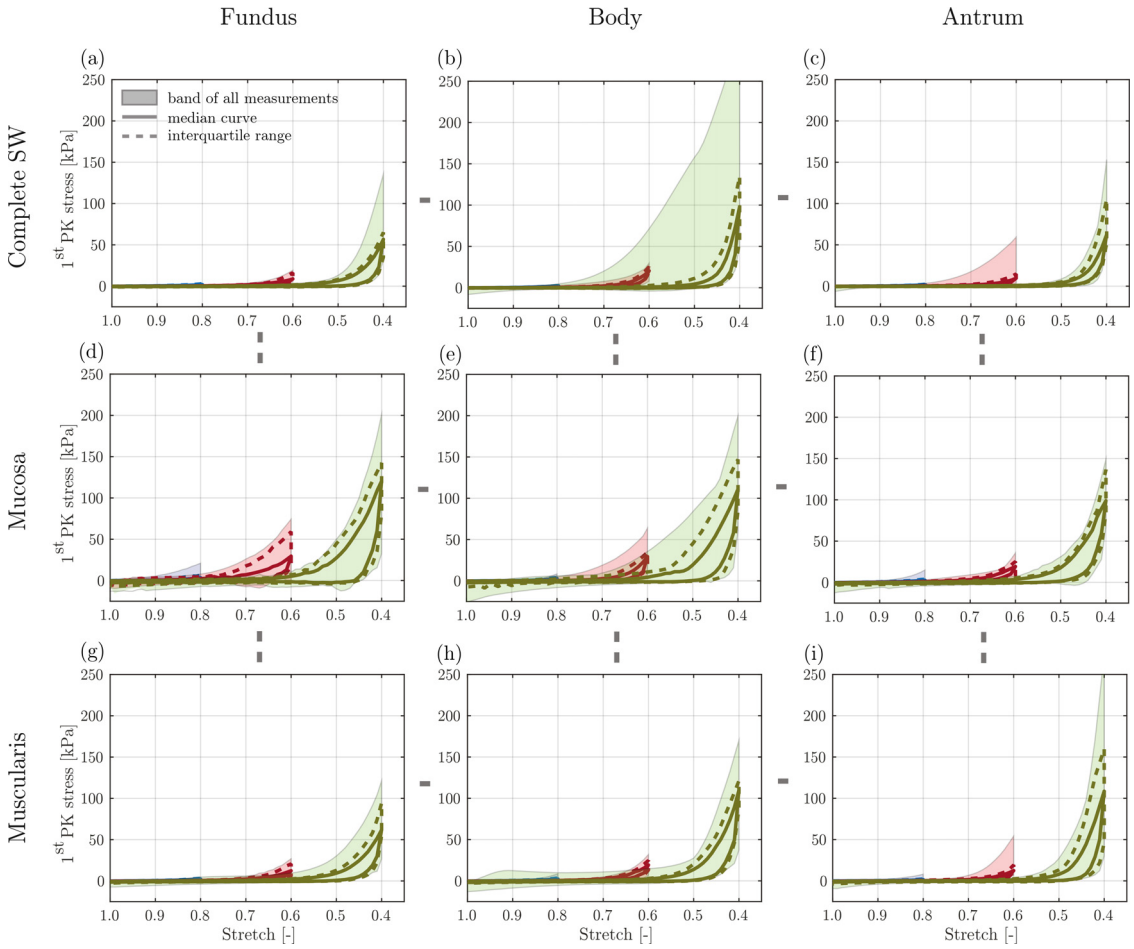

Fig. 9. Region- and layer-dependent stress-strain behavior during the last cycles of quasi-static radial compression loading with $\lambda = \{0.8, 0.6, 0.4\}$. Blue, red, and green solid curves describe the median tissue response to maximum radial compression of 20%, 40%, and 60%, respectively. The dashed curves represent the interquartile range of the data and the shaded areas include all measurement curves. A total of $n = 10$ samples per test condition were considered.

markable that only the single layers of the body showed a slight directional dependence. While the mucosa showed a higher mechanical response in the circumferential direction ($p < 0.14$), the muscularis experienced higher shear stresses along the longitudinal direction ($p < 0.21$). In general, all samples showed a linear behavior up to about 30% shear, followed by an exponential increase in the stress-strain curve.

3.6. Stress-relaxation tests

The formation of hysteresis during the quasi-static mechanical tests suggested a strong viscoelastic behavior of the SW (see Fig. S5 for the evaluation of the hysteresis area of all quasi-static loading modes). Therefore, stress-relaxation tests were conducted in radial compression and simple shear mode, each for several maximum strains, to get more information about the viscoelasticity of stomach tissue.

3.6.1. Radial compression

The results of the radial compression tests showed that the maximum level of relaxation and the steepness of the slope of immediate relaxation increased with the level of radial compression (Fig. 11). Within each region and for each compression level, the muscularis and the complete SW showed similar stress-time behavior. In each region, the mucosa relaxed the most (although not statistically significant), followed by the muscularis and the complete SW (fundus: $p < 0.39$; body: $p < 0.06$; antrum: $p < 0.69$). The mucosa of all regions also showed a pronounced difference in slope and maximum relaxation between $\lambda = 0.8$ and $\lambda = 0.6$ ($p < 0.02$), and only a small divergence between the curves from $\lambda = 0.6$ and $\lambda = 0.4$ in all regions ($p < 0.46$). Similar behavior was observed for the muscularis and complete SW of the body ($p < 0.02$). Antral relaxation measurements showed large differences between the tested layers for $\lambda = \{0.8, 0.6\}$ ($p < 0.31$) and their rather similar behavior for $\lambda = 0.4$ ($p > 0.38$).

The level of relaxation after 10 min showed a higher variability between the single measurements at lower strains, see Fig. 11(d)–(f). At higher levels of compression, the measurements show a relaxation of over 90% for all layers and regions. As expected, the peak stresses and their variability increased with increasing compression, see Fig. 11(g)–(i). Within the fundus, the mucosa experienced the highest peak stresses for all compression levels, followed by the complete SW and the muscularis ($p < 0.08$). Within the body and antrum, the mucosa showed the greatest peak stresses for $\lambda = \{0.8, 0.6\}$ (body: $p < 0.26$; antrum: $p < 0.37$), while $\lambda = 0.4$ showed the stiffest peak response throughout the complete SW (body: $p < 0.01$; antrum: $p < 0.57$).

3.6.2. Simple shear tests

The results of the samples sheared up to 20% and 40% diverged only minimally in their maximum relaxation and average peak shear stress, but not in their region and layer-specific behavior, see Fig. 12 and S6. Compared to the mechanical response to radial compression, all samples subjected to shear stress relax-

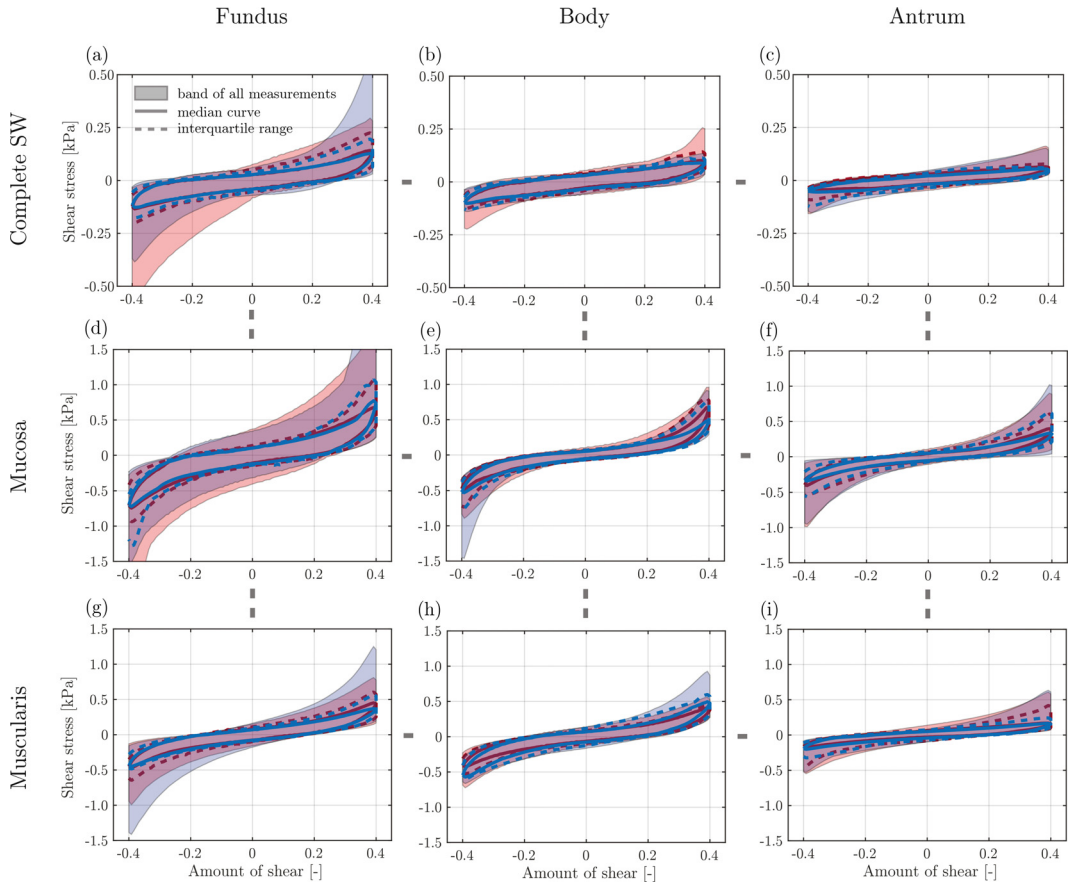

Fig. 10. Region-, layer-, and orientation-dependent stress-strain behavior during the last cycle of quasi-static shear loading with $\gamma = 0.4$. Red and blue solid curves represent the median of the tissue response to longitudinal and circumferential shear, respectively. The dashed curves represent the interquartile range of the data and the shaded areas include all measurement curves. A total of $n = 10$ samples per testing condition were considered.

ation experienced a lower level of relaxation after a waiting period of 10 min. While the fundus and body tissues showed similar maximum relaxation levels, the antrum relaxed considerably less ($p < 0.31$). In all regions, the muscularis and the complete SW presented similar stress-time curves. In contrast to the results of the quasi-static tests, the body and the antrum showed very little directional anisotropy (complete SW: $p > 0.21$; single layers: $p > 0.42$). The single layers of the fundus, on the other hand, presented slight differences between the circumferential and longitudinal directions (muscularis: $p < 0.19$; mucosa: $p < 0.39$).

The degree of maximum relaxation of the fundus samples differed between the layers depending on the amount of shear. At 20% shear, the complete SW relaxed the most, followed by the mucosa and muscularis, whose mechanical response was quite similar. However, at a shear of 40%, the mucosa showed the highest relaxation. In the body and antrum, the complete SW relaxed the most at both shear strains (except longitudinal at 40% shear) ($p < 0.14$). While the mucosa in the body relaxed more than the muscularis, the opposite was the case in the antrum.

The peak shear stress and its variability increased with the amount of shear applied to the sample, see Fig. 12(g)–(i). Similar to radial compression, the fundus experienced the highest peak stresses, followed by the body and the antrum ($p < 0.19$). Within the fundus, the single layers showed a similar and statistically significantly stiffer mechanical response than the complete SW ($p < 0.01$). A layer-specific difference in peak shear stress was also observed in the body, where the mucosa and the muscularis responded more strongly than the complete SW at both 20% and 40% shear ($p < 0.01$). In contrast to the fundus, the peak shear stresses for both single layers were not the same. At 20% shear the muscularis behaved slightly more stiffly and at 40% shear the mucosa experienced higher peak stresses. In the antrum, the mucosal layer showed the highest shear stresses, followed by the muscularis and the complete SW ($p < 0.01$).

4. Discussion

4.1. Microstructure of the stomach wall

To gain insight into the microstructure of the porcine SW, a rather uncommon staining protocol was introduced. Specifically, Elastica van Gieson was combined with Alcian blue. This special combination enabled the differentiation of collagen fibers, muscle fibers, cell nuclei and mucus on a tissue slide. Importantly, the combination of both stains proved successful for each stomach region, allowing for a clear structural analysis within each of its layers (Figs. 5 and 6).

The detailed microstructural analysis turned out to be crucial for understanding the mechanics of biological tissues in general [61] and the stomach wall in particular, see Sections 4.2 and 4.3. The histology of the porcine stomach reported in this study shows no clear deviation from the literature. In particular, a strong regional variation in the complete SW and the single-layer thickness (Section 3.1) is in agreement with Zhao et al. [31], Bauer et al. [39], Park et al. [62], and Friis et al. [37]. Ross and Pawlina [63] and Bauer et al. [39] have also reported on the numerous accumulations of fat found mainly, but not exclusively, in the fundic submucosa. The differences in the alignment of the mucinous glands in the stomach region also agree with the literature [22,47,63]. The variation in the stratum arrangement of the muscularis was also

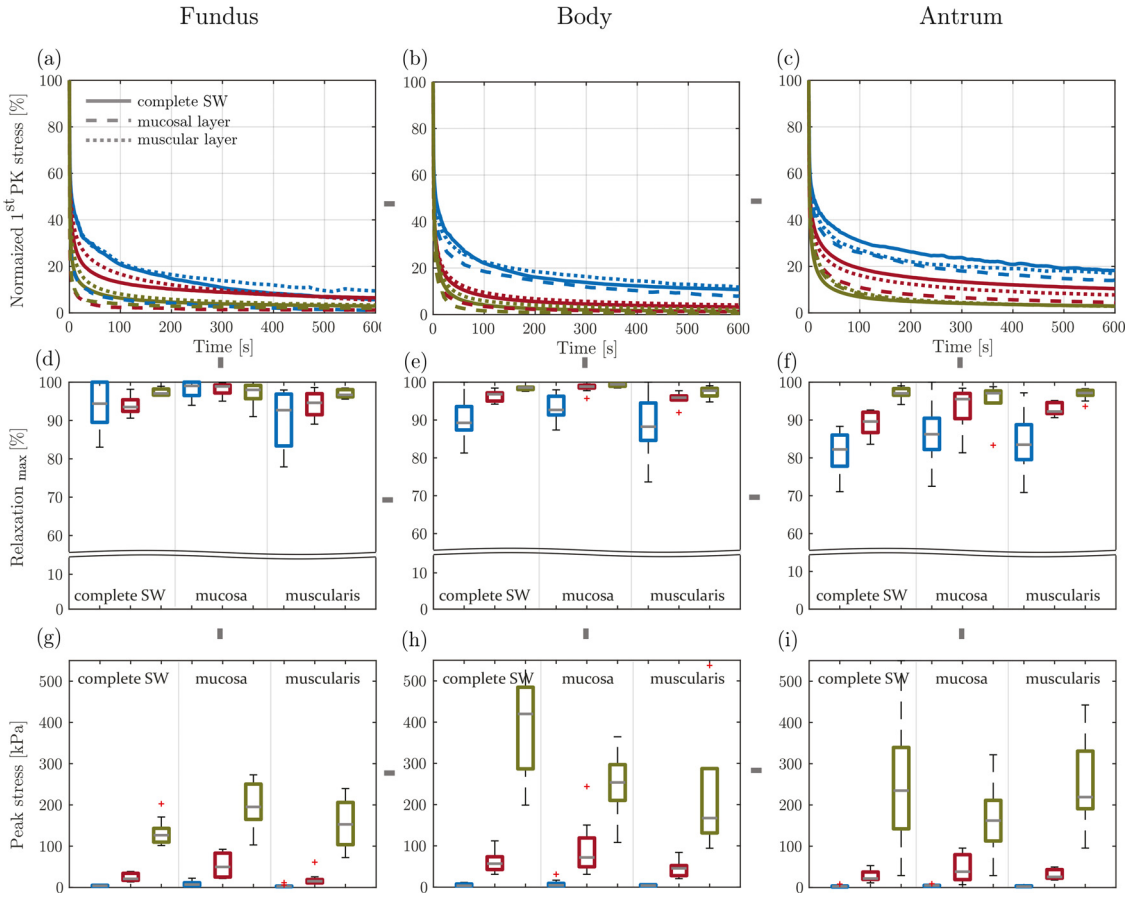

Fig. 11. Region- and layer-dependent relaxation tests in radial compression. In (a)–(c), the blue, red, and green curves describe the median of the normalized first Piola-Kirchhoff stress versus relaxation time for maximum radial compression of 20%, 40% and 60%, respectively. The solid, dashed, and dotted curves depict the response of the complete SW, mucosa, and muscularis, respectively. From this, box plots (d)–(f) for the stress relaxation after 10 min and (g)–(i) for the peak stresses were extracted. The box plots follow the same color coding as the relaxation curves and depict the median, upper and lower quartile, and maximum and minimum values. A total of $n = 10$ samples per test condition were considered.

reported for the porcine stomach by Bauer et al. [39], and for the rat stomach by Natale et al. [64].

4.2. Mechanical behavior of the stomach wall

In agreement with previous studies [38,39], the mechanical response of porcine stomach tissue revealed strong nonlinearity and viscoelasticity. Both the viscous and the elastic response presented a high degree of regional and layer-specific differences, while the mechanical anisotropy during tensile and shear tests was only observed at higher strain rates.

4.2.1. Preconditioning behavior

Sample preconditioning was conducted for each quasi-static loading mode to achieve a stable and repeatable mechanical tissue response. While this pre-measurement step is often applied to biological tissue, there are currently only loose recommendations and no standardized protocols. In general, the maximum strain and strain rate of the preconditioning step should match the actual measurement [65,66] and the number of preconditioning cycles should be chosen so that the deviation between two consecutive loading and unloading curves becomes a minimum [66,67].

Based on those recommendations, different numbers of preconditioning cycles were tested during preliminary studies. For the planar biaxial extension, 5 cycles were found to be sufficient. A comparison with the literature highlights the nonconformity in gastric tissue preconditioning during stretch experiments. The number of preconditioning cycles ranges from zero [30,34,39] to 2 [31,33] up to a maximum of 7 cycles [38]. Similar to the biaxial tests, preliminary studies on the preconditioning behavior during shear and radial compression tests were conducted. While only 2 preconditioning cycles were required for the shear experiments, 5 were necessary for the radial compression tests. Although the compressive and shear loading of internal organs is of great importance in medical procedures, to the best of the authors' knowledge, no such studies have been conducted and published on stomach tissue subjected to shear deformation and only one on radial compression, where 3 preconditioning cycles were applied [37]. For other internal organs, the recommended number of preconditioning cycles varies between 0 [68] and 2 [49,69] in shear and from 0 [29,70] over 2 [69], up to 20 [71] in compression. In each of the mechanical tests, significant tissue softening was observed between the first and second preconditioning cycle. This change in response is consistent with previous mechanical studies of the GI tract [31,33,38,72].

In general, in the field of biomechanics, it is still a matter of debate whether the preconditioned tissue response represents a true equilibrium state and how it should relate to the physiology of an organ. Preconditioning effects rarely occur *in vivo*. However, this study should lay the foundation for a material model that depicts the purely passive tissue behavior. Therefore, the preconditioning of the gastric tissue had no impact on the mechanical response obtained or on the representativeness of the resulting material properties.

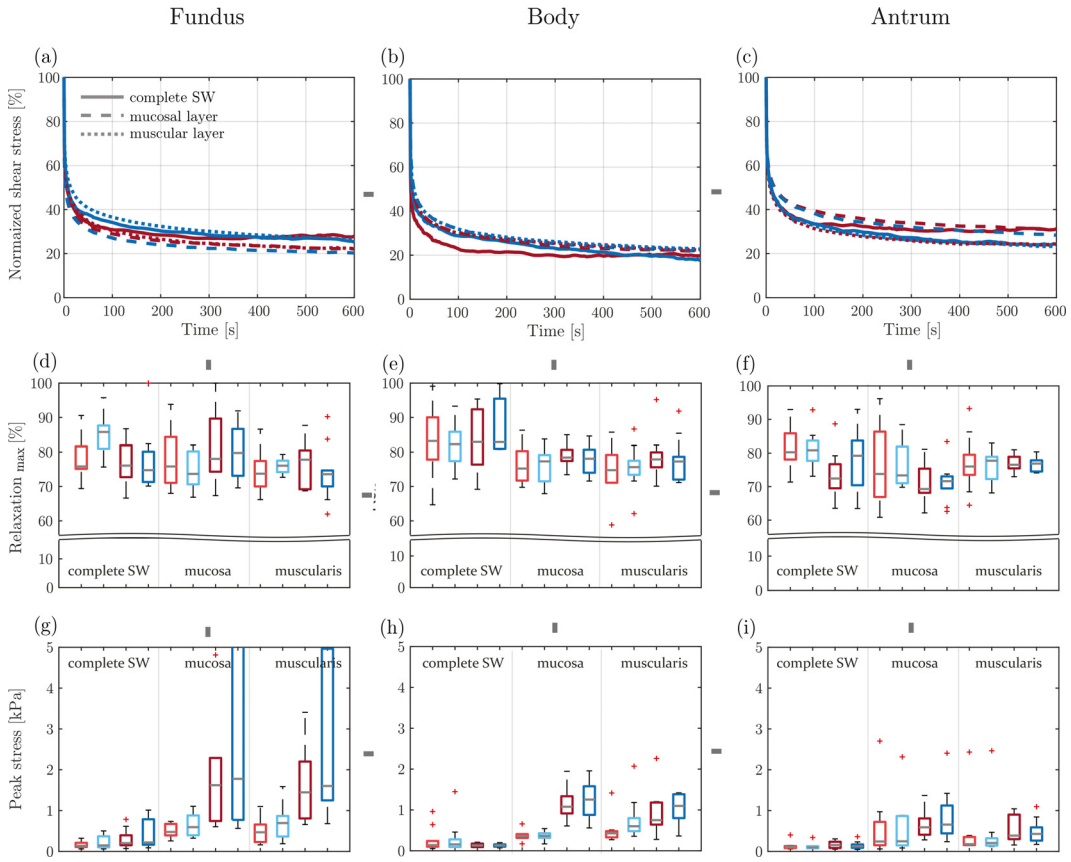

Fig. 12. Region-, layer-, and orientation-dependent relaxation tests in shear mode with $\gamma = \{0.2, 0.4\}$. In (a)–(c), the red and blue curves describe the median of the normalized shear stress versus relaxation time for the maximum amount of shear of $\gamma = 0.4$ in the longitudinal and circumferential directions, respectively. The solid, dashed, and dotted curves depict the response of the complete SW, mucosa, and muscularis, respectively. From this, the box plots (d)–(f) for stress relaxation after 10 min, and (g)–(i) for peak stresses were extracted. The box plots follow the same color coding as the relaxation curves. Furthermore, in (d)–(i), the lighter shades depict the tissue response at $\gamma = 0.2$, while the darker ones show the behavior at $\gamma = 0.4$. A total of $n = 10$ samples per test condition were considered.

4.2.2. Biaxial extension testing

To estimate the regional and layer-dependent anisotropy of porcine gastric tissue, biaxial extension tests up to tissue failure were performed. Similar to the study by Aydin et al. [38], the samples from fundus, body and antrum could be stretched up to a maximum of $\lambda_{\text{max-eval}} = \{1.4, 1.2, 1.3\}$, respectively (see Table 2).

Comparable to Zhao et al. [31], of all layers tested, the mucosa achieved the highest stresses and the lowest stretches until failure in the fundus and the body, but not in the antrum. This observation could be explained by the differences in the alignment of the gastric glands between the antrum and the body or fundus (see Section 3.1). Also comparable to Zhao et al. [31], the muscularis showed the highest stresses and ruptured before the other two layers in antral samples. Even if the comparison with the study of Bauer et al. [39] suggests something different at first glance, the definition of the so-called pre-stretch of the research group [39] must be taken into account. This pre-stretch was introduced to consider the sampling history, such as the unfolding of the mucosal layer, and resulted in a shift in its measurements. Without this factor, their specified yield stretches [39] were very similar to the maximum stretches obtained in our study. Importantly, the biaxial extension experiments of our study were conducted on substantially smaller samples compared to [38,39]. This made it possible to test only areas where mucosal folding was negligible. This enabled us to prevent possible pre-stretching due to tissue sampling.

In the case of planar biaxial extension, the mechanical anisotropy was only observed at the highest achieved stretches, which varied strongly between regions and layers, see Fig. 8. In general, the largest differences between the two stretching directions were observed in the muscularis. While the antral muscular layer was stiffer along the circumferential direction, the muscularis of the fundus and body was stiffer along the longitudinal direction. This can be explained by the microstructure of the stomach. The longitudinal stratum of the muscularis is particularly pronounced in the fundus and proximal part of the body and thins towards the antrum (see Section 3.1). For the circumferential stratum, it was the other way around. Within the muscularis, muscle bundles are enveloped by collagen sheets. The thicker a certain stratum, the more collagen fibers are aligned towards the direction of the stratum and the stiffer the tissue response becomes.

The mucosa of any region did not show a pronounced degree of directional anisotropy, consistent with its more radially oriented microstructure. However, the antral mucosa presented slight differences between the circumferential and longitudinal directions, possibly due to an insufficient number of samples or the underlying microstructure. It is noteworthy that, unlike the glands of the body and fundus, the glands of the antrum are mainly tortuous and clustered by collagen and muscle fibers.

Mechanical anisotropy was also observed throughout the complete SW, but to a much lesser degree than within the muscular layer. Interestingly, the complete SW in the fundus behaved softer along the longitudinal direction and the complete SW samples of the body and antrum showed a stiffer response along the longitudinal direction. While the anisotropy of the complete SW agrees with the anisotropy of the muscular layer in the body region, it

shows the opposite behavior in the fundus and antrum. Since the mucosal layer exhibits a rather isotropic behavior, the different response could be influenced by the submucosa. In this regard, previous studies have shown that when the complete SW is stretched, most of the mucosa unfolds, while the thick submucosa thins due to planar stretch [39,62]. Another possible explanation for this phenomenon could lie in the regional functions during digestion. While the fundus must also expand in the longitudinal direction during uptake of food for gas storage, the body and antrum are responsible for accommodating the chyme through minimal circumferential expansion during subsequent digestion steps [73,74]. The complete SW should not experience a drastic stress increase due to the described digestion mechanisms [24,75], which could lead to a more compliant response along the main direction of expansion for each region. A mechanical anisotropy of the muscularis and the complete SW was also found by other research groups [31,37,39]. Consistent with our results, the previous studies reported a stiffer behavior of the muscularis of the fundus and body as well as of the complete SW of the body and the antrum along the longitudinal direction. In contrast to our study, the antral muscular layer and the complete SW of the fundus did not show any softer behavior along the circumferential direction.

4.2.3. Radial compression testing

During surgical interventions, the SW is often compressed by staples, sutures, or other surgical equipment that hold the tissue in place [76]. A thorough understanding of the tissue response to radial compression is therefore of utmost importance. To the best of the authors' knowledge, this is the first time that systematic radial compression tests featuring multiple compression levels have been performed on passive stomach tissue. In particular, the studies carried out so far only included one level of compression and did not ensure a passive response [29,37].

Interestingly, the complete SW displayed the softest behavior, followed by the muscularis and mucosa for each region during radial compression. In other words, the result of the complete SW is not the mean result of the mucosal and muscular layers. It can therefore be assumed that the submucosa plays a key role in bearing radial loads. The results may suggest that first the loosely interconnected submucosa is packed into a denser form before the majority of the load-bearing fibers are recruited and further extended within the circumferential-longitudinal plane (perpendicular to the compression loading direction).

For each region, the mucosa exhibited the stiffest behavior of the three layer combinations tested, which at first seemed counterintuitive. It is noteworthy, however, that the mucosa consists of mucus-filled glands (Fig. 6), which are usually sealed with glue and sandpaper during radial compression. In biological tissue, fibers are supposed to ensure strength under tensile and shear loading, while the matrix material, which is commonly characterized by a high water content, such as mucus, stabilizes the tissue in order to withstand compressive loading [77]. The high mucus content along with sealed glands could therefore explain the stiff mechanical response of the mucosa. Furthermore, the complete SW of the body, which contains the largest proportion of mucosa in the total tissue thickness (Fig. 5), shows a stiffer tissue response compared to the fundus and antrum.

The muscularis samples showed a stiffer response in the antrum and body compared to the fundus. A possible explanation for this phenomenon could lie in their microstructure. The longitudinal and circular strata of the fundus are of equal thickness and were reported to have a wavy structure [39]. However, the muscularis of the body and antrum is dominated by the circular stratum. Unlike the muscular layer of the body and antrum, the strata of the fundus are flattened and densely packed before the load-bearing fibers are recruited. The delayed fiber recruitment might result in a softer response.

It is noteworthy that the higher stresses measured in the complete SW and the muscularis were reported by Friis et al. [37]. In contrast to our study, tissue was tested fresh, stored in a saline solution prior to testing, and only sprayed with Krebs solution during testing, which may have resulted in partial reactivation of smooth muscle fibers. The test environment and the reactivation of smooth muscle fibers could therefore be the reason for the generally higher measured stresses in the complete SW and the muscularis. However, in agreement with the present study, the mucosa and the complete SW in the body behaved stiffest of all gastric regions [37]. In addition, Rosen et al. [29] reported the nominal stress of the SW, which was about four times higher than the results of the present study. This stiffer response could also be influenced by the test environment and the reactivation of the smooth muscle fibers since the experiments were conducted in air, at room temperature, and on the entire organ [29]. In the case of stomach tissue, this means that the internal folds of the mucosa at the test site and the ratio of reactivated smooth muscle cells are unknown, which could strongly affect the total thickness and lead to a misleading tissue response. The at least partial reactivation of the smooth muscle fibers in the tissue is very probable, since the tissue tested by Rosen et al. [29] showed a stiffening between the first and fifth loading cycle. Finally, the nominal stresses obtained in the radial compression tests on the complete wall of the large intestine agree well with the present study [70].

4.2.4. Simple shear testing

Shear effects within and between layers are ubiquitous in the SW, e.g., during digestion of food and also during surgical procedures as a side effect of compression and cutting with medical equipment. However, shear tests of stomach tissue tend to be underrepresented in biomechanical studies of the GI tract. In order to close this gap, simple shear tests up to different maximum strains were conducted as part of this study.

Although some mechanical anisotropy was expected based on the structural anisotropy and the layered structure of the SW, little to none was observed. Only the median curves of the mucosa and muscularis in the body showed slight differences between the stress-strain curves in the longitudinal and circumferential directions. While the mucosa behaved slightly stiffer in the circumferential direction, the muscularis showed a somewhat stiffer behavior in the longitudinal direction. However, both cases showed a rather isotropic interquartile range, suggesting that a larger number of samples could affect the median curves.

Of all three regions, the antrum responded most gently to shear strain. The fundus, on the other hand, experienced the stiffest response. This phenomenon can be explained by regional functionality. During digestion, the trapped gases are stored in the fundus [78] and in the two distal regions of the stomach, i.e. the body and the antrum, the chyme is ground down by peristaltic movements of the wall [79], which, through interaction with solid food components, leads to shear forces that are exerted on the SW. These shear forces are indented to send signals to mechanosensitive cells that control the digestive process and should not lead to damage within the SW [80]. The mechanical properties of the body and antrum might therefore evolve to follow this function and ensure low shear forces in these two distal stomach regions.

Compared to the single layers, the complete SW showed a significantly lower stiffness. This could be due to the strong influence of the collagen fiber network of the submucosa and serosa, whose main role is to reduce potential friction within and between the layers. The muscularis experienced the second lowest shear stress, possibly due to the influence of the partially present serosal layer. Considering the high water content of the mucus and the low

amount of collagen fibers in the mucosal layer, it seems counter-intuitive that it showed the stiffest behavior under shear stresses. A potential explanation could lie in the composition of the mucus. Among other things, it consists of about 95% water, mucin secretions (glycoproteins), proteoglycans, and lipids [81]. Importantly, the glycoproteins form networks that cause the mucus to exhibit higher viscosity at low shear rates and a Newtonian behavior at increased shear rates [77].

4.2.5. Time-dependent behavior

The conducted stress-relaxation experiments in radial compression and shear support the common understanding that GI tissues behave viscoelastic. Consistent with our observations, multiple previous studies reported a strong time dependency of the tissue response [29,33,35–37,82].

The radial compression relaxation tests suggested that out of the three layer combinations the mucosa relaxed the most within 10 min (see Fig. 11). Interestingly, the mucosa of the antrum showed less relaxation, possibly due to the collagen-enveloped glandular accumulations. In most cases, however, the tissue relaxed between 80% and 95%. Such a high degree of relaxation could also indicate a restructuring or even damage to the glandular ducts and not an actual tissue relaxation into its (almost) reference configuration.

In contrast to the generally high level of relaxation in the present study, Rosen et al. [29] found a level of relaxation of only 10% to 15% of the stomach after 60 s. However, the group conducted relaxation tests *in vivo* on the whole organ. The difference in the results between [29] and the present study can therefore be explained by the combination of a possible smooth muscle reactivation, the lateral confinement of the surrounding organ, and the tested bi-layer including a possible flattening of mucosal rugae. Nevertheless, the level of relaxation, the magnitude of the peak stresses, and the general stress-time evolution reported by Friis et al. [37] are consistent with the findings in the present study. Consistent with our observations, the study [37] revealed that the mucosa in the fundus relaxed more than in the two distal gastric regions, and that the complete SW in the two proximal regions relaxed more than in the antrum within 2.5 min. Both the fundus and the body took less time to reach their relaxed equilibrium state than the antrum, both in the [37] and in the present study. However, it should be noted that the study [37] presented fewer layer and region-dependent deviations compared to our experiments.

In the radial compression tests, the difference in peak stress between quasi-static and relaxation experiments increased for the complete SW and decreased for the mucosal layer with the maximum strain applied. On average, the maximum stress during the relaxation tests for all three compression levels and all region-layer combinations was twice that in the quasi-static mode (compare Figs. 9 with 11(g)–(i)). Against this background it should be noted that a strong regional dependency of the peak stress during the radial compression of the different layers was observed.

The maximum stress relaxation in step tests was generally higher in radial compression than in shear. In contrast to the radial compression results, the difference in maximum stress between quasi-static and relaxation experiments did not increase with the applied maximum strain. The peak stress during the relaxation tests was approximately twice that in the quasi-static mode for both shear strains and all region-layer combinations. Comparable to the quasi-static tests, a slight directional anisotropy was found in the relaxation test. This observation suggests that the directional, regional, and layer-specific tissue response to shear strain does not depend on the strain rate but only on the maximum stress. In general, the tissue relaxes between 70% and 80% with little difference between the two maximum shear strains.

Although no studies reported shear tests on stomach tissue, Li et al. [82] conducted shear step tests on passive porcine intestines, which are microstructurally similar to gastric tissue. Measurements on the complete intestinal wall showed a similar peak force, albeit with a lower maximum relaxation than the present study. The measurements obtained lasted only 10 s [82], therefore the lower maximum relaxation could continue to increase after 10 min, resulting in a stress-time curve similar to ours.

Similar to the present study, Carniel et al. [35] could not find any significant difference in the relaxation behavior between the circumferential and the longitudinal direction in step tests with uniaxial extension of the human stomach. Loading along both directions resulted in a similar level of relaxation and stress-time evolution, resulting in a sharp immediate decay within the first few seconds, followed by a slow convergence towards equilibrium. Friis et al. [36] conducted frequency-dependent uniaxial tensile tests on samples of the porcine complete SW. Similarly to the present study, not only the regional variations, but also the differences between the tissue response in circumferential and longitudinal direction were investigated. Contrary to the present study they found the fundus to have the softest response followed by the body and antrum, which behaved comparably stiff. While little to no directional anisotropy was found in the storage and loss modulus of the fundus, both were higher in the longitudinal direction of the body and antrum samples at each testing frequency.

4.3. Functionality in relation to the mechanical response

When assessing the stomach response to mechanical loading, the region- and layer-specific gastric functionality should be considered. While shear stresses are always present in this multi-layered tissue during digestion [83] and in interaction with other organs in the abdominal cavity, planar extension and radial compression of the SW are not physiological loading conditions. It is a common misconception that the SW is stretched to accommodate food when in reality the increase of the volume during digestion is largely due to smooth muscle relaxation and flattening of the otherwise folded mucosa overlying the loosely connected submucosa, leading to greater compliance and more degrees of freedom [73,84,85]. The fact that both planar extension and radial compression are not physiological loading conditions could explain why extension and compression tests required more preconditioning cycles and were exposed to higher stresses compared to shear tests. Due to peristaltic movements and the interplay between SW and chyme, interlayer shear stresses are constantly present and are of crucial importance for mechanosensing during the digestive process [86–89].

Besides chyme storage, the main components of gastric motility are mixing and emptying [20,90,91]. These motor functions take place in the distal stomach, i.e., the body and in the antrum. During the mixing phase, the chyme combines with gastric juices and the solid content is broken down by peristaltic movements of the muscularis [92]. The circumferential stratum of the muscularis is mainly responsible for the grinding process during digestion [90,93]. This is also consistent with the microstructure of the stomach [39,64] (see also Fig. 5(b)–(c) and Fig. 6(g) and (k)), with the proportion of the circumferential stratum within the body and antrum being significantly greater than that of the longitudinal stratum and increasing steadily towards the pylorus.

After the grinding phase, the chyme is passed to the intestines for further digestion and absorption [75]. The process of gastric emptying is highly complicated and is controlled by powerful cyclic antral contraction waves that push the chyme through the pylorus. The pyloric sphincter prevents food particles larger than 1–2 mm from moving towards the duodenum and propels them back into the stomach. This phenomenon leads to consider-

able shear forces between the mucosa and the solid food particles in the distal stomach, which further reduce the particle size [94]. The role of the distal mucosa in gastric emptying also correlates with the results of the present study, i.e., with the substantially lower mucosal response to shear in the body and antrum than in the fundus (see Fig. 10(d)–(f)).

4.4. Influence of sex

To investigate possible associations between sex and biomechanical tissue response and microstructure, half of the sacrificed pigs were male and half were female. While the measures of the entire stomachs varied according to the sex of the animal, showing significantly larger and heavier male organs (Table 1), the experimental results of the mechanical tests showed no statistically relevant dependence on the sex of the animal. Also histology indicated no difference in the composition of the gastric microstructure between the male and female pigs. However, it must be noted that this may not be the case in human gastric tissue, where differences in motility during digestion have been reported [95–98]. Therefore, a follow-up study on human gastric tissue should include both male and female subjects to investigate possible sex dependencies.

4.5. Future directions

While basic research is vital in itself, it should benefit society and consider potential applications, particularly in the field of biomechanics. An obvious application of gastric mechanics is in surgical interventions. Since simulations of surgical interventions require a reliable material model, the logical next step would be to estimate a suitable constitutive model. In this context, we focused on the microstructure in the reference configuration by analyzing two-dimensional histological slides of the three stomach regions. However, as a crucial next step, the three-dimensional distribution of the main components (e.g., collagen and muscle fibers) in the reference configuration should be examined and quantified, as well as the change in their orientation and distribution in response to mechanical loading. This could help gain a more comprehensive understanding of the interplay between mechanics, structure and functionality of gastric tissue and provide structural parameters for material modeling. In addition, an analogous biomechanical study of human tissue would be of great importance. In particular, it should be essential to estimate whether preclinical studies on pigs are sufficient with regard to human physiology or whether a material model used in a medical context should be based exclusively on human tissue.

5. Conclusion

In the present study, we have successfully reported experimental results on porcine stomach tissues obtained from three different loading modes, i.e., multi-ratio planar biaxial extension, simple shear in two orthogonal directions, and radial compression. In order to document the highly viscoelastic behavior of the gastric tissue, experiments were conducted in quasi-static and in the relaxation mode. The biomechanical tests were performed on the three main regions of the stomach and for the complete SW as well as the separated mucosa and muscular layer. This strategic testing approach resulted in an unprecedented, extensive mechanical data set reflecting the region, layer, and directional differences of this tissue. The mechanical tests were accompanied by histological examinations that highlighted the very heterogeneous microstructure of the porcine stomach and explained differences in its mechanical behavior. This comprehensive data set can be used to gain further insights into this complex multi-layered tissue and its response to various loading conditions, which might help improve existing treatments or develop surgical approaches for gastric pathologies. In addition, the study provides a solid basis for creating viscoelastic material model that accounts for the layer- and region-dependent variation of SW.

Declaration of Competing Interest

The authors declare that they have no known competing financial interests or personal relationships that could have appeared to influence the work reported in this paper.

Acknowledgements

This work was funded by Covidien LP. The authors thank Oliver Kugler and Harald Gassner for assistance with the experimental testing and repetitive laboratory tasks required to conduct the study.

Supplementary material

Supplementary material associated with this article can be found, in the online version, at 10.1016/j.actbio.2023.11.008.

References

[1] N. O'Morain, C. O'Morain, The burden of digestive disease across Europe: facts and policies, Digestive Liver Dis. 51 (2019) 1–3.
[2] A.F. Peery, S.D. Crockett, C.C. Murphy, E.T. Jensen, H.P. Kim, M.D. Egberg, J.L. Lund, A.M. Moon, V. Pate, E.L. Barnes, C.L. Schlusser, T.H. Baron, N.J. Shaheen, R.S. Sandler, Burden and cost of gastrointestinal, liver, and pancreatic diseases in the United States: update 2021, Gastroenterol. 162 (2022) 621–644.
[3] U.S. Department of Health and Human Services and National Institutes of Health, 2009, Opportunities & Challenges in Digestive Diseases Research: Recommendations of the National Commission on Digestive Diseases. NIH Publication.
[4] A.F. Peery, E.S. Dellon, J. Lund, S.D. Crockett, C.E. McGowan, W.J. Bulsiewicz, L.M. Gangarosa, M.T. Thiny, K. Stizenberg, D.R. Morgan, Y. Ringel, H.P. Kim, M.D. DiBonaventura, C.F. Carroll, J.K. Allen, S.F. Cook, R.S. Sandler, M.D. Kappelman, N.J. Shaheen, Burden of gastrointestinal disease in the United States: 2012 update, Gastroenterol. 143 (2012) 1179–1187.
[5] A.F. Peery, S.D. Crockett, C.C. Murphy, J.L. Lund, E.S. Dellon, J.L. Williams, E.T. Jensen, N.J. Shaheen, A.S. Barritt, S.R. Lieber, B. Kochar, E.L. Barnes, Y.C. Fan, V. Pate, J. Galanko, T.H. Baron, R.S. Sandler, Burden and cost of gastrointestinal, liver, and pancreatic diseases in the United States: update 2018, Gastroenterol. 156 (2019) 254–272.
[6] B. Stierman, J. Afful, M.D. Carroll, T.-C. Chen, O. Davy, S. Fink, C.D. Fryar, Q. Gu, C.M. Hales, J.P. Hughes, Y. Ostchega, R.J. Storandt, L.J. Akinbami, National health and nutrition examination survey 2017–March 2020 prepandemic data files-Development of files and prevalence estimates for selected health outcomes, National Health Statistics Reports 158 (2021).
[7] Z.J. Ward, S.N. Bleich, M.W. Long, S.L. Gortmaker, Association of body mass index with health care expenditures in the United States by age and sex, PLoS ONE 16 (2021) e0247307.
[8] F.X. Pi-Sunyer, Comorbidities of overweight and obesity: current evidence and research issues, Med. Sci. Sports Exerc. 31 (1999) 602–608.
[9] Y. Lim, J. Boster, Obesity and Comorbid Conditions, StatPearls Publishing, 2022.
[10] M. Ilic, I. Ilic, Epidemiology of stomach cancer, World J. Gastroenterol. 28 (2022) 1187–1203.
[11] E. Morgan, M. Arnold, M.C. Camargo, A. Gini, A.T. Kunzmann, T. Matsuda, F. Meheus, R.H.A. Verhoeven, J. Vignat, M. Laversanne, J. Ferlay, I. Soerjomataram, The current and future incidence and mortality of gastric cancer in 185 countries, 2020-40: a population-based modelling study, EClinicalMedicine 47 (2022) 101404.
[12] H.-O. Adami, D. Hunter, D. Trichopoulos, Textbook of Cancer Epidemiology, Oxford University Press, 2008.
[13] P.R. Schauer, D.L. Bhatt, J.P. Kirwan, K. Wolski, S.A. Brethauer, S.D. Navaneethan, A. Aminian, C.E. Pothier, E.S.H. Kim, S.E. Nissen, S.R. Kashyap, Bariatric surgery versus intensive medical therapy for diabetes - 3-year outcomes, N. Engl. J. Med. 370 (2014) 2002–2013.
[14] G. Mingrone, S. Panunzi, A. De Gaetano, C. Guidone, A. Iaconelli, G. Nanni, M. Castagneto, S. Bornstein, F. Rubino, Bariatric–metabolic surgery versus conventional medical treatment in obese patients with type 2 diabetes: 5 year follow-up of an open-label, single-centre, randomised controlled trial, Lancet 386 (2015) 964–973.
[15] M. Sasako, M. Saka, T. Fukagawa, H. Katai, T. Sano, Surgical treatment of advanced gastric cancer: Japanese perspective, Dig. Surg. 24 (2007) 101–107.
[16] E.V. Cutsem, X. Sagaert, B. Topal, K. Haustermans, H. Prenen, Gastric cancer, Lancet 388 (2016) 2654–2664.

[17] National Health Commission of the People's Republic of China, Chinese guidelines for diagnosis and treatment of gastric cancer 2018 (English version), Chin. J. Cancer Res. 31 (2019) 707–737.
[18] V. Nováček, T.N. Tran, U. Klinge, R.H. Tolba, M. Staat, D.G. Bronson, A.M. Miesse, J. Whiffen, F. Turquier, Finite element modelling of stapled colorectal end–to-end anastomosis: advantages of variable height stapler design, J. Biochem. 45 (2012) 2693–2697.
[19] I. Toniolo, C.G. Fontanella, M. Gagner, C. Stefanini, M. Foletto, E.L. Carniel, Computational evaluation of laparoscopic sleeve gastrectomy, Updates Surg. 73 (2021) 2253–2262.
[20] V. Mahadevan, Anatomy of the stomach, Surgery 35 (2017) 608–611.
[21] L.W. Lamps (Ed.), Diagnostic Pathology: Normal Histology, Amirsys Publishing, 2013.
[22] C.E. Mackintosh, L. Kreel, Anatomy and radiology of the areae gastricae, Gut 18 (1977) 855–864.
[23] A.D. Keet (Ed.), The Pyloric Sphincteric Cylinder in Health and Disease, Springer Science & Business Media, 1993.
[24] S. Brandstaeter, S.L. Fuchs, R.C. Aydin, C.J. Cyron, Mechanics of the stomach: a review of an emerging field of biomechanics, GAMM Mitt. 42 (2019) e201900001.
[25] D. Liao, J. Zhao, H. Gregersen, Regional surface geometry of the rat stomach based on three-dimensional curvature analysis, Phys. Med. Biol. 50 (2005) 231–246.
[26] D. Liao, J. Zhao, H. Gregersen, A novel 3D shape context method based strain analysis on a rat stomach model, J. Biomech. 45 (2012) 1566–1573.
[27] E.L. Carniel, A. Frigo, C.G. Fontanella, G.M. De Benedictis, A. Rubini, L. Barp, G. Pluchino, B. Sabbadini, L. Polese, A biomechanical approach to the analysis of methods and procedures of bariatric surgery, J. Biomech. 56 (2017) 32–41.
[28] C.G. Fontanella, C. Salmaso, I. Toniolo, N. deCesare, A. Rubini, G.M. deBenedictis, E.L. Carniel, Computational models for the mechanical investigation of stomach tissues and structure, Ann. Biomed. Eng. 43 (2019) 1237–1249.
[29] J. Rosen, J.D. Brown, S. De, Biomechanical properties of abdominal organs in vivo and postmortem under compression loads, J. Biomech. Eng. 130 (2008) 021020.
[30] V.I. Egorov, I.V. Schastlivtsev, E.V. Prut, A.O. Baranov, R.A. Turusov, Mechanical properties of the human gastrointestinal tract, J. Biomech. 35 (2002) 1417–1425.
[31] J. Zhao, D. Liao, P. Chen, P. Kunwald, H. Gregersen, Stomach stress and strain depend on location, direction and the layered structure, J. Biomech. 41 (2008) 3441–3447.
[32] R.N. Miftahof, H.G. Nam, Mathematical Foundations and Biomechanics of the Digestive System, Cambridge University Press, 2010.
[33] Z.G. Jia, W. Lin, Z.R. Zhou, Mechanical characterization of stomach tissue under uniaxial tensile action, J. Biomech. 48 (2015) 651–658.
[34] G. Rotta, J. Kobiela, S. Grymek, M. Karczewska, Mechanical properties of the human stomach under uniaxial stress action, Curr. Sci. 116 (2019) 1886–1893.
[35] E.L. Carniel, A. Albanese, C.G. Fontanella, P.G. Pavan, L. Prevedello, C. Salmaso, S. Todros, I. Toniolo, M. Foletto, Biomechanics of stomach tissues and structure in patients with obesity, J. Mech. Behav. Biomed. Mater. 110 (2020) 103883.
[36] S.J. Friis, T.S. Hansen, M. Poulsen, H. Gregersen, J.V. Nygaard, Dynamic viscoelastic properties of porcine gastric tissue: effects of loading frequency, region and direction, J. Biomech. 143 (2022) 111302.
[37] S.J. Friis, T.S. Hansen, M. Poulsen, H. Gregersen, A. Brõel, J.V. Nygaard, Biomechanical properties of the stomach: a comprehensive comparative analysis of human and porcine gastric tissue, J. Mech. Behav. Biomed. Mater. 138 (2023) 105614.
[38] R.C. Aydin, S. Brandstaeter, F.A. Braeu, M. Steigenberger, R.P. Marcus, K. Nikolaou, M. Notohamiprodjo, C.J. Cyron, Experimental characterization of the biaxial mechanical properties of porcine gastric tissue, J. Mech. Behav. Biomed. Mater. 74 (2017) 499–506.
[39] M. Bauer, E. Morales-Orcajo, L. Klemm, R. Seydewitz, V. Fiebach, T. Siebert, M. Bņl, Biomechanical and microstructural characterisation of the porcine stomach wall: location- and layer-dependent investigations, Acta Biomater. 102 (2020) 83–99.
[40] C. Schmid, Techniken der extrakorporalen zirkulation, in: P. Feindt, F. Harig, M. Weyand (Eds.), Empfehlungen zum Einsatz und zur Verwendung der Herz-Lungen-Maschine, Steinkopff Verlag, Darmstadt, 2006, pp. 309–315.
[41] F.A. Hensley, D.E. Martin, G.P. Gravlee (Eds.), A Practical Approach to Cardiac Anesthesia, Lippincott Williams & Wilkins, 2012.
[42] C.S. Packer, M.L. Kagan, J.F. Kagan, S.A. Robertson, N.L. Stephens, The effect of 2,3-butanedione monoxime (BDM) on smooth muscle mechanical properties, Pflügers Arch. – Eur. J. Physiol. 412 (1988) 659–664.
[43] A. Oesterman, A. Arner, U. Malmqvist, Effects of 2,3-butanedione monoxime on activation of contraction and crossbridge kinetics in intact and chemically skinned smooth muscle fibres from guinea pig taenia coli, J. Muscle Res. Cell Motil. 14 (1993) 186–194.
[44] K. Brixius, R.H.G. Schwinger, Modulation of cross-bridge interaction by 2,3-butanedione monoxime in human ventricular myocardium, Naunyn Schmiedebergs Arch. Pharmacol. 361 (2000) 440–444.
[45] R.S. Kirton, A.J. Taberner, P.M. Nielsen, A.A. Young, D.S. Loiselle, Effects of BDM, $[Ca^{2+}]$*bibkey*1_o, and temperature on the dynamic stiffness of quiescent cardiac trabeculae from rat, Am. J. Physiol. Heart Circ. Physiol. 288 (2005) H1662–H1667.
[46] G. Sommer, T.C. Gasser, P. Regitnig, M. Auer, G.A. Holzapfel, Dissection properties of the human aortic media: an experimental study, J. Biomech. Eng. 130 (2008). 021007–1–12
[47] K. Leus, G.P. Goodall, A.A. Macdonald, Anatomy and histology of the babirusa (Babyrousa babyrussa) stomach, C. R. Acad. Sci. Paris, Sciences de la vie 322 (1999) 1081–1092.
[48] G. Sommer, M. Eder, L. Kovacs, H. Pathak, L. Bonitz, C. Mueller, P. Regitnig, G.A. Holzapfel, Multiaxial mechanical properties and constitutive modeling of human adipose tissue: a basis for preoperative simulations in plastic and reconstructive surgery, Acta Biomater. 9 (2013) 9036–9048.
[49] G. Sommer, A.J. Schriefl, M. Andrä, M. Sacherer, C. Viertler, H. Wolinski, G.A. Holzapfel, Biomechanical properties and microstructure of human ventricular myocardium, Acta Biomater. 24 (2015) 172–192.
[50] A. Pukaluk, H. Wolinski, C. Viertler, P. Regitnig, G.A. Holzapfel, G. Sommer, Changes in the microstructure of the human aortic medial layer under biaxial loading investigated by multi-photon microscopy, Acta Biomater. 151 (2022) 396–413.
[51] W. Sun, M.S. Sacks, M.J. Scott, Effects of boundary conditions on the estimation of the planar biaxial mechanical properties of soft tissues, J. Biomech. Eng. 127 (2005) 709–715.
[52] A. Eilaghi, J.G. Flanagan, G.W. Brodland, C.R. Ethier, Strain uniformity in biaxial specimens is highly sensitive to attachment details, J. Biomech. Eng. 131 (2009) 0910031–0910037.
[53] S. Budday, G. Sommer, C. Birkl, C. Langkammer, J. Haybaeck, J. Kohnert, M. Bauer, F. Paulsen, P. Steinmann, E. Kuhl, G.A. Holzapfel, Mechanical characterization of human brain tissue, Acta Biomater. 48 (2017) 319–340.
[54] C. Bellini, P. Glass, M. Sitti, E.S.D. Martino, Biaxial mechanical modeling of the small intestine, J. Mech. Behav. Biomed. Mater. 4 (2011) 1727–1740.
[55] G. Sommer, D.C. Haspinger, M. Andrä, M. Sacherer, C. Viertler, P. Regitnig, G.A. Holzapfel, Quantification of shear deformations and corresponding stresses in the biaxially tested human myocardium, Ann. Biomed. Eng. 43 (2015) 2234–2348.
[56] J.A. Niestrawska, C. Viertler, P. Regitnig, T.U. Cohnert, G. Sommer, G.A. Holzapfel, Microstructure and mechanics of healthy and aneurysmatic abdominal aortas: experimental analysis and modeling, J. R. Soc. Interface 13 (2016) 20160620.
[57] G.A. Holzapfel, Nonlinear Solid Mechanics. A Continuum Approach for Engineering, John Wiley & Sons, Chichester, 2000.
[58] P.A. Kelly, Solid Mechanics Part I: An introduction To Solid mechanics, Solid Mechanics Lecture Notes, University of Auckland, 2013.
[59] F.T. Bosman, P. Yan (Eds.), Pathobiology of Human Disease, Elsevier Publishing, 2014.
[60] J. Feher (Ed.), Quantitative Human Physiology, Elsevier Publishing, 2017.
[61] S. Cranford, M.J. Buehler, Materiomics: biological protein materials, from nano to macro, Nanotechnol. Sci. Appl. 3 (2010) 127–148.
[62] S. Park, H.J. Chun, Y.D. Kwon, B. Keum, Y.S. Seo, Y.S. Kim, Y. Jeen, S.H. Um, C.D. Kim, H.S. Ryu, J.H. Lee, Y. Chae, Stretching causes extensive changes of gastric submucosa: is it acceptable to define 500 μm as the safe margin? Gut Liver 2 (2008) 199–204.
[63] M.H. Ross, W. Pawlina, Histology: A Text and Atlas: with Correlated Cell and Molecular Biology, 6th ed., Lippincott Williams & Wilkins, 2011.
[64] M.R.D. Natale, L. Patten, J.C. Molero, M.J. Stebbing, B. Hunne, X. Wang, Z. Liu, J.B. Furness, Organisation of the musculature of the rat stomach, J. Anat. 240 (2022) 711–723.
[65] Y.C. Fung, Biomechanics. Mechanical Properties of Living Tissues, 2nd ed., Springer-Verlag, New York, 1993.
[66] S. Cheng, E.C. Clarke, L.E. Bilston, The effects of preconditioning strain on measured tissue properties, J. Biomech. 42 (2009) 1360–1362.
[67] N. Conza, Part 3: tissue preconditioning: engineering issues in experimental biomedicine series, Exp. Tech. 29 (2006) 43–46.
[68] F. Ahmad, R. Prabhu, J. Liao, S. Soe, M.D. Jones, J. Miller, P. Berthelson, D. Enge, K.M. Copeland, S. Shaabeth, R. Johnston, I. Maconochie, P.S. Theobald, Biomechanical properties and microstructure of neonatal porcine ventricles, J. Mech. Behav. Biomed. Mater. 88 (2018) 18–28.
[69] S. Budday, G. Sommer, J. Haybaeck, P. Steinmann, G.A. Holzapfel, E. Kuhl, Rheological characterization of human brain tissue, Acta Biomater. 60 (2017) 315–329.
[70] M. Higa, Y. Luo, T. Okuyama, T. Takagi, Y. Shiraishi, T. Yambe, Passive mechanical properties of large intestine under in vivo and in vitro compression, Med. Eng. Phys. 29 (2006) 840–844.
[71] J. Yang, L. Yu, L. Wang, W. Wang, J. Cui, The estimation method of friction in unconfined compression tests of liver tissue, J. Eng. Med. 41 (2018) 3441–3447.
[72] C. Durcan, M. Hossain, G. Chagnon, L. Perić, D. Bsiesy, G. Karam, E. Girard, Experimental investigations of the human oesophagus: anisotropic properties of the embalmed muscular layer under large deformation, Biomech. Model. Mechanobiol. 21 (2022) 1169–1186.
[73] S. Banerjee, A. Pal, M. Fox, Volume and position change of the stomach during gastric accommodation and emptying: a detailed three-dimensional morphological analysis based on MRI, Neurogastroenterol. Motil. 32 (2020).
[74] M. Bleeker, M.C.C.M. Hulshof, A. Bel, J.-J. Sonke, A. van der Horst, Gastric deformation models for adaptive radiotherapy: personalized vs population-based strategy, Radiother. Oncol. 166 (2022) 126–132.
[75] R.K. Goyal, Y. Guo, H. Mashimo, Advances in the physiology of gastric emptying, Neurogastroenterol. Motil. 31 (2019).
[76] R. Huang, M. Gagner, A thickness calibration device is needed to determine staple height and avoid leaks in laparoscopic sleeve gastrectomy, Obesity Surg. 25 (2015) 2360–2367.

[77] J. Vincent, Structural biomaterials, Princeton University Press, Princeton, 2012.
[78] H. Fritsch, W. Kőhnel, Taschenatlas Anatomie Innere Organe, Thieme Verlag, 2005.
[79] R. Klinke, H.-C. Pape, A. Kurtz, S. Silbernagl, Physiologie, Thieme Verlag, 2009.
[80] A. Beyder, In pursuit of the epithelial mechanosensitivity mechanisms, Front. Endocrinol. (Lausanne) 9 (2019).
[81] O.A. Ohar, J.F. Donohue, S. Spangenthal, The role of guaifenesin in the management of chronic mucus hypersecretion associated with stable chronic bronchitis: a comprehensive review, Chronic Obstr. Pulm. Dis. 6 (2019) 341–349.
[82] J. Li, X. Bi, K. Zhang, C. Zhang, H. Liu, Experimental study on the effects of shear stress on viscoelastic properties of the intestines, Sci. China Technol. Sci. 62 (2019) 1028–1034.
[83] Y. Li, F. Kong, Simulating human gastrointestinal motility in dynamic in vitro models, Compr. Rev. Food Sci. Food Saf. 21 (2022) 3804–3833.
[84] T. Arakawa, H. Uno, T. Fukuda, K. Higuchi, K. Kobayashi, T. Kuroki, New aspects of gastric adaptive relaxation, reflex after food intake for more food: involvement of capsaicin-sensitive sensory nerves and nitric oxide, J. Smooth Muscle Res. 33 (1997) 81–88.
[85] H.P. Parkman, M.P. Jones, Tests of gastric neuromuscular function, Gastroenterology 136 (2009) 1526–1543.
[86] G.J. Mahler, M.B. Esch, R.P. Glahn, M.L. Shuler, Characterization of a gastrointestinal tract microscale cell culture analog used to predict drug toxicity, Biotechnol. Bioeng. 104 (2009) 193–205.
[87] M. Chi, B. Yi, S. Oh, D.J. Park, J.H. Sung, S. Park, A microfluidic cell culture device (muFCCD) to culture epithelial cells with physiological and morphological properties that mimic those of the human intestine, Biomed. Microdevices 17 (2015).
[88] A. Mercado-Perez, A. Beyder, Gut feelings: mechanosensing in the gastrointestinal tract, Nat. Rev. Gastroenterol. Hepatol. 19 (2022) 283–296.
[89] A. Sontheimer-Phelps, D.B. Chou, A. Tovaglieri, T.C. Ferrante, T. Duckworth, C. Fadel, V. Frismantas, A.D. Sutherland, S. Jalili-Firoozinezhad, M. Kasendra, E. Stas, J.C. Weaver, C.A. Richmond, O. Levy, R. Prantil-Baun, D.T. Breault, D.E. Ingber, Human Colon-on-a-chip enables continuous in vitro analysis of colon mucus layer accumulation and physiology, Cell. Mol. Gastroenterol. Hepatol. 9 (2020) 507–526.
[90] F. Kong, R.P. Singh, Disintegration of solid foods in human stomach, J. Food Sci. 73 (2008).
[91] A.R. Hobson, Q. Aziz, Oesophagus and stomach motility, Medicine 39 (2006) 210–213.
[92] K.A. Kelly, Gastric emptying of liquids and solids: roles of proximal and distal stomach, Am. J. Physiol. 239 (1980) 651–658.
[93] W. Schwizer, A. Steingoetter, M. Fox, Magnetic resonance imaging for the assessment of gastrointestinal function, Scand. J. Gastroenterol. 41 (2006) 1245–1260.
[94] W. Liu, Y. Jin, P.J. Wilde, Y. Hou, Y. Wang, J. Han, Mechanisms, physiology, and recent research progress of gastric emptying, Crit. Rev. Food Sci. Nutr. 61 (2020) 2742–2755.
[95] F.L. Datz, P.E. Christian, J. Moore, Gender-related differences in gastric emptying, J. Nucl. Med. 28 (1987) 1204–1207.
[96] L.P. Degen, S.F. Phillips, Variability of gastrointestinal transit in healthy women and men, Gut 39 (1996) 299–305.
[97] L.C. Knight, H.P. Parkman, K.L. Brown, M.A. Miller, D.M. Trate, A.H. Maurer, R.S. Fisher, Delayed gastric emptying and decreased antral contractility in normal premenopausal women compared with men, Am. J. Gastroenterol. 92 (1997) 968–975.
[98] B. Mearadji, C. Penning, M.K. Vu, P.J. van der Schaar, A.S. van Petersen, I.M. Kamerling, A.A. Masclee, Influence of gender on proximal gastric motor and sensory function, Am. J. Gastroenterol. 96 (2001) 2066–2073.